geosciences

MDPI

Article

Petrographic and Textural Characterization of Beach Sands Contaminated by Asbestos Cement Materials (Cape Peloro, Messina, Italy): Hazardous Human-Environmental Relationships

Roberta Somma

Department of Mathematical and Computer Sciences, Physical Sciences and Earth Sciences, University of Messina, Viale F. Stagno d'Alcontres 31, Sant'Agata, 98166 Messina, Italy; rsomma@unime.it

Abstract: In the past fifteen years, the contamination of the Italian marine coastal environments by asbestos cement materials (ACMs) represents a known crux mostly reported or denounced by mass media and environmental associations. A recent research reporting compositional and textural data related to ACMs found in the beach deposits of a protected natural reserve (Cape Peloro, Messina, Italy) induced the author to perform new petrographic and textural analyses on the Cape Peloro beach sands, pebbles, cobbles (BSPC), and technofossils (bricks, tails, slab, concrete), associated with the previously studied ACMs, in order to compare the data with those of the ACMs previously reported in the literature. The petrographic investigations allowed the author to determine that beach sands and weakly gravelly sands were characterized by a quartzo–lithic signature, being mainly composed of metamorphic grains of quartz (50–60%) and metamorphic lithics (40–50%, mainly composed of polymineral quartz + microcline, quartz + plagioclase, quartz + biotite, quartz + muscovite grains, and monomineral opaque minerals, plagioclase, k-feldspar, and almandine garnet grains), whereas the pebbles and cobbles were made of acid intrusive (granitoids) and metamorphic rocks (gneiss, augen gneiss prevailing). Pebbles and cobbles made up of porphyroids could derive from the cannibalization of the underlying lower to middle Pleistocene siliciclastic deposits of the Messina Formation. Differently, the gneiss, augen gneiss, and granitoids forming the beach pebbles and cobbles, being present both in the crystalline rocks of the Aspromonte Unit and in the clasts of the SGMF, could originate from both of them. Textural investigations allowed the author to characterize grain size, shape parameters, and roundness in the beach deposits. These were mostly composed of sands and weakly gravelly sands with medium grains. Parameters, such as elongation and flatness, showed higher values in the BSPC than in the technofossils. The shapes of the BSPC were mostly from oblate to equant, whereas the shapes of the technofossils were mostly from bladed to oblate. The main differences depended on the original shape of the technofossils, being mostly platy, and their softer composition. The roundness was from angular to sub-rounded. In the Ionian coast of the Cape Peloro peninsula, the source areas for the well-rounded ACM found on the beach and in the beach deposits could have at least four different origins: (i) Possible landfills widespread since the 1970s in the intensively urbanized coastal areas. (ii) Direct abandonment in the coastal area. (iii) Direct abandonment in the streams. (iv) Activities to counteract the erosion/lack of sediment using non-conforming materials. Considering the diffused damage caused by the coastal erosion affecting most of the Italian coast and the obvious increasing dispersion of the asbestos fibers from the ACMs over time, effectual counter actions to prevent further contamination and guidelines for clean-up efforts are necessary.

Keywords: Mediterranean Sea; Pleistocene siliciclastic sediments; beach deposits; petrofacies; texture; coastal area contamination; asbestos cement materials; technofossils

Citation: Somma, R. Petrographic and Textural Characterization of Beach Sands Contaminated by Asbestos Cement Materials (Cape Peloro, Messina, Italy): Hazardous Human-Environmental Relationships. *Geosciences* **2024**, *14*, 167. https://doi.org/10.3390/geosciences14060167

Academic Editors: Jesus Martinez-Frias and Pierre Rochette

Received: 2 May 2024
Revised: 5 June 2024
Accepted: 11 June 2024
Published: 14 June 2024

1. Introduction

Credit for reporting the first cases of the contamination of marine coastal and fluvial environments by asbestos cement materials (ACMs) must be given to Italian mass media

and environmental associations. Indeed, for at least fifteen years, journalists and environmental associations, such as Legambiente and the Worldwide Fund for Nature (WWF Italy), have reported tens of beaches contaminated by ACMs, from northern to southern Italy, along the Tyrrhenian, Ionian, and Adriatic coasts of the Mediterranean Sea [1–20], along rivers, such as the Po River in the Padana plain [21], or the countryside [22]. Until today, notwithstanding this alarming press news, scientific research devoted to this key issue still seems to be very scarce. Indeed, it is only in these last years that two distinct groups of Italian researchers have reported their independent data on the ACMs contamination of coastal areas [23,24].

The effectual research of Lisco et al. [23] mainly consisted of a sedimentological, geomorphological, and remote-sensing investigation at the beach of Marechiaro Bay (Taranto, southern Italian peninsula), aiming to identify the provenance of the ACMs and the evolution of the study area due to erosion and accretion phenomena. The provenance of the ACMs was identified in a landfill of construction and demolition wastes present in the surroundings of the studied beach.

Analogous approaches and methods, used by Somma et al. [24] on the beaches of the Cape Peloro peninsula (Messina, southern Italy, north coast of the island of Sicily), provided similar results. Indeed, the search for fibers in the ACM allowed the researchers to identify diffused asbestos mineral fibers [24]. This research was mainly devoted to the mineralogical composition and texture of the ACMs as well as to evidence the extension of the contaminated beach area. Provenances of ACMs from both onshore and offshore areas were also ascertained. The stratified encrustations of marine organisms on previous continental organisms recognized on the ACMs allowed the researchers to demonstrate that part of the ACMs was transported from the submerged beach to the beach and vice versa, after their littoral drift as material composing the sedimentary supply delivered by the streams or local illegal landfills eroded by the wave action. Evidence of these fragments was also observed in the stratigraphic layers of the beach sands excavated by the sea waves during the storm events [24]. The entity of the evidenced criticism was also much more serious with respect to the research of Lisco et al. [23], Cape Peloro being a protected area. Over 520 fragments of ACMs were identified on the Cape Peloro beaches, along a transect 4500 m long, stretching from the Tyrrhenian to the Ionian Sea. The percentage of ACMs found in the Ionian coast was higher than in the Tyrrhenian coast [24].

Considering the high recreational and touristic values of the Italian coasts, due to their extension (the sandy and gravel beaches are about 3270 km long) [25] and favorable climate of the Mediterranean type, today, the ACMs contamination of the Italian coastal areas represents a new challenge and an alarming criticism, for the consequent and potentially hazardous human-environment interactions responsible for health and environmental risks. Indeed, asbestos fibers (chrysotile, crocidolite, amosite, actinolite, anthophyllite, and tremolite), which may be delivered in the air by asbestos cement, may be hazardous minerals, if inhaled, causing mesothelioma. The asbestos cement, present in corrugated roofings, water tanks and tubes, insulation, and textile materials, was produced by industries beginning in the early-mid-19th century. In the 1990s, the Italian law n. 257 of 1992 banned the production and use of asbestos cement because of its toxicity and consequent high health hazard, but remnants of these materials are still widespread in the Italian territory [24].

With this in mind, the present research was aimed to (i) deepen the knowledge of the petrographic and textural features of the modern beach sands, pebbles, cobbles, and technofossils (sensu "reserved remnants of human technology" [26]) collected at Cape Peloro, in order to compare their characteristics with those previously analyzed in the ACMs [24], (ii) further hypothesize the ACM origin in the beaches, and (iii) attract interest to the serious health and environmental risks that hazardous wastes, such as ACMs, may cause.

2. Study Area

The study area is localized in the spit–peninsula of Cape Peloro, one of the widest marine coastal plains of the Messina town extending along the northeastern coast of the island of Sicily (Figure 1).

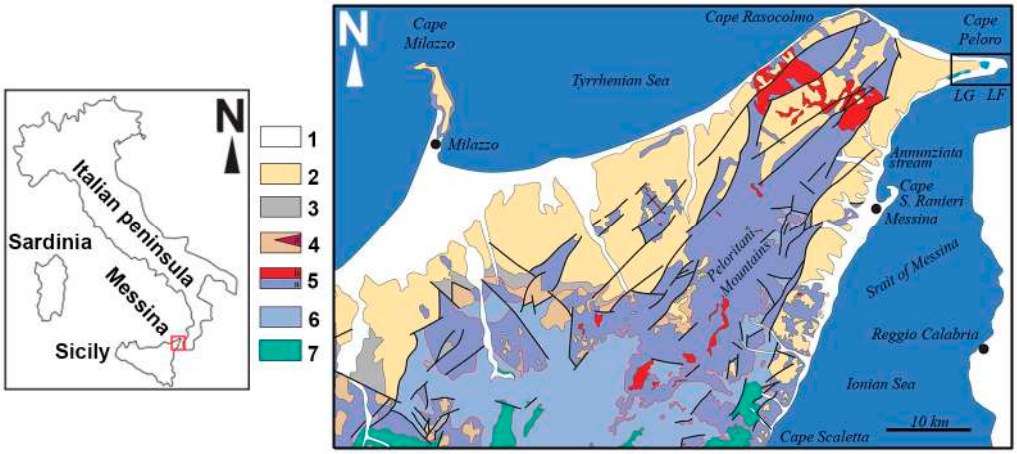

Figure 1. Geological sketch map of the NE sector of the Peloritani Mountains (NE Sicily). The black rectangle on the Cape Peloro peninsula (NE edge of Messina) evidences the sector of the coast studied (see Figure 2). In this peninsula, the Cape Peloro lagoon area (coastal lakes in sky blue color) is formed by Lake Ganzirri (LG) and Lake Faro (LF). Legend: (1) Alluvial and beach deposits (Holocene). (2) Miocene–Pleistocene sedimentary successions (including the Pleistocene Messina Fm). (3) Floresta calcarenites (Langhian–upper Burdigalian) and Antisicilide Complex (lower Miocene-upper Cretaceous). (4) Stilo–Capo d'Orlando Formation (Burdigalian) with olistoliths (a). (5) Aspromonte Unit (a: Variscan metamorphic basement; b: Plutonic basement). (6) Mela Unit (Variscan metamorphic basement). (7) Mandanici–Piraino Unit (Variscan metamorphic basement and Mesozoic cover). The red square on the insert on the left represents the extension of the geological sketch map. The map was modified after [27].

Cape Peloro has high environmental, recreational, and touristic valences.

The environmental value of Cape Peloro was recognized beginning in 1972, when the Cape Peloro Lagoon (Figure 1) was included in the UNESCO Water Project, as a site of naturalistic importance. For the presence of the brackish coastal lakes of Ganzirri and Faro (Figure 1) in the area, two geosites of Mondial interest for morphotectonics were instituted by the Sicilian region. For their environmental value, Cape Peloro was protected, becoming a natural reserve (Natural Oriented Reserve of Cape Peloro) and, at the same time, it was introduced as a protected zone of the Nature 2000 network (Special Protection Zone—SPZ, SPZ ITA030042—Monti Peloritani, Dorsale Curcuraci, Antennamare, and marine area of the Straits of Messina—27,993 he [28]; partially overlapping the SPZ ITA030008—Capo Peloro—Ganzirri Lakes—60 he [29]).

The great recreational and touristic values of the Cape Peloro beaches are attributed by Italian and foreign bathers to the beauty and crystallinity of the waters (where dolphins and sperm whales may be sighted), the monuments (Mazzone, Torre degli Inglesi, and Torre Saracena), the attraction of the tallest electricity pylon, the cultural foundations, the scuba diving, the sport centers, the resorts, and the catering activities. "Historical" beaches, such as those of the Mortelle and Torre Faro villages, are until today among the most crowded for the Messina citizens and foreign tourists. Finally, the peculiar morphology of the cape, being a spit–peninsula facing both into the Tyrrhenian and Ionian Seas, represents another significatively appreciated value for its unique landscape beauty and legends. For this reason, in 2022, the *American Journal of the National Geographic* rewarded Cape Peloro among the 12 most beautiful Italian beaches, ranking it first as the best for views [30].

3. Geological Setting

Cape Peloro forms the NE tip of the Peloritani Mountains (Figure 1). The Peloritani Alpine Chain extends from this cape to the Taormina–Sant'Agata tectonic line, forming the SE ends of the Calabria–Peloritani Arc [27,31,32]. The chain is composed of a thrust pile, sealed by thrust–top deposits, middle–upper Burdigalian in age. Most of these tectonic units are formed by Variscan crystalline basements, preserving remnants of original Mesozoic–Cenozoic sedimentary covers. These thrust sheets are formed as follows, from top to base: the Aspromonte, Mela, Mandanici–Piraino, Alì–Montagnareale, Fondachelli, and Longi–Taormina Units [17,31,32]. The upper units (Aspromonte and Mela Units) are affected by a Variscan high- to medium-grade metamorphism, whereas the lower units (Mandanici–Piraino, Fondachelli, and Longi–Taormina Units) are affected by a Variscan medium- to very low-grade metamorphism, from top to base of the thrust pile [17,31,32]. An Alpine overprint was also recognized in the Aspromonte and Mandanici–Piraino Units [33–35], whereas an anchizone metamorphism affected the post-Varican sedimentary sequence of the Alì–Montagnareale Unit [36].

The strong post-orogenic uplift of the Calabria–Peloritani Arc originated significative source areas submitted to erosion and consequent transport and deposition of consistent amounts of siliciclastic rocks, mostly composed of metamorphic and igneous rocks. The main Miocene to Holocene siliciclastic sequences of the Peloritani Mountains are, from base to top, as follows:

i. The Stilo–Capo d'Orlando Fm (middle–upper Burdigalian). The unit is composed of a syn- to late-tectonic terrigenous sequence made up of sandy, sandy–clayey, and sandy–conglomeratic turbidites, with olistoliths of metamorphic and sedimentary rocks. Clasts of the conglomerates were mostly composed of metamorphic rocks (gneiss, schists, phyllites) [37], quartz, and granitoids.
ii. The San Pier Niceto Fm (Tortonian to lower Messinian). The unit is formed by sandstones, siltstones, marly and sandy–clayey alternations, marls, clayey marls, and conglomerates. Clasts of the conglomerates were mostly composed of metamorphic rocks, often with platy shapes [38].
iii. The Messina Fm (lower to middle Pleistocene). The unit is made up of sands and gravels locally with moderately cemented layers. Clasts of the gravels were mostly composed of metamorphic rocks (gneiss, augen gneiss), quartz, granitoids, and pinkish or grayish porphyroids [38].
iv. The beachrocks (upper Holocene [39]). Clasts of the conglomerates were made up of crystalline rocks (granitoids and high-grade metamorphic rocks).

The hills surrounding Cape Peloro are mostly composed of the crystalline basement of the Aspromonte Unit (Figure 1). This tectonic unit is made up of amphibolite facies Palaeozoic rocks with late to post-Hercynian peraluminous intrusive bodies, locally overprinted by Alpine age metamorphism, developed about 25–30 Ma ago along deep-seated shearing zones [35,40]. In the study area, the unit is in tectonic contact with the Messina Fm by means of the active extensional Messina Fault System [41].

The Cape Peloro connects the E–W trending Tyrrhenian Sea to the ENE–WSW trending Ionian Sea, through the Messina Strait. Along the cape, the orientation of the coast gradually evolves from E–W in the Tyrrhenian side to NE–SW in the cape and ENE–WSW in the Ionian side. This latter orientation depends on morphotectonic phenomena related to the WSW–ENE-trending capable normal fault system of Scilla–Ganzirri [41], shaping the northern end of the Messina Strait. The strait coasts formed during the last 16 ky, as a consequence of the complex interactions between the post-Wurmian sea-level rise and the extensional tectonics characterizing this sector of the Calabria–Peloritani Arc [41–43]. The Cape Peloro area originated during the Late Pleistocene–Holocene time span. The stratigraphy of the peninsula is composed of continental siliciclastic layers (middle Upper Holocene), from 7 to 30 m thick [39], overlying in unconformity a substrate made up of beachrocks [39,43]. Beachrocks consist of carbonate-cemented materials formed rapidly (within a few hundred years) within the intertidal zone on warm temperate to tropical

coasts [44]. These rocks are exposed in the nearshore of Cape Peloro, along an extensive shore-parallel belt extending for tens of kms, from Mortelle in the Tyrrhenian coast to the Port of Messina on the Ionian side. The Cape Peloro beachrocks are 5.9 ka old and are present mostly between 0.70 m a.s.l. and the isobath −2 m [43]. After their genesis, the beachrocks were drowned by sea-level rise, remaining partially under shallow waters partially covered by the modern shore deposits [41]. These latter are composed of sands with pebbles and cobbles, deriving from metamorphic and igneous source rocks. The thickness, measured in the drillings carried out for the Messina bridge project, should be ≤60 m [42]. The age of these deposits is younger than 5.9 ka [39,43].

4. Wave Climate and Sediment Littoral Drift

In Sicily, the regional plan for the management of hydrogeology and coasts subdivided the coasts into 21 coastal physiographic units (CPU), delimited by the main prominent capes [45–48]. Each CPU is a sediment coastal cell, localized in a specific sector of the coast and characterized by a sediment littoral drift occurring in the same unit without significant sediment exchanges with other adjacent units.

The Cape Peloro (Figure 2a) peninsula hosts wave-dominated sandy beaches (Figure 2b) subject to significative marine coastline migration during the different seasons. The coastal plain deposits essentially originated from the stream mobile supplies, partially remodeled by the action of the sea.

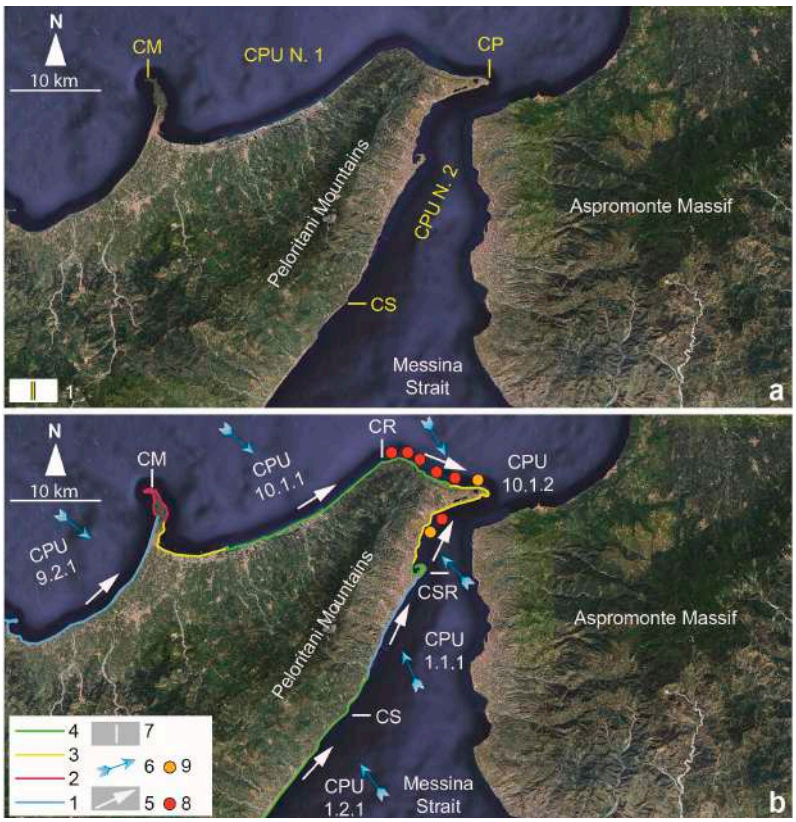

Figure 2. CPUs in the NE edge of Sicily. (**a**) Cape Peloro falls between two CPUs, n. 1 and 2 [45]. (**b**) Cape Peloro falls in the III order CPU Cape Rasocolmo-Cape San Ranieri (n. 10.1.2) [48]. Legend. (**a**) 1: Limit between CPUs [45]. (**b**) 1: Low pebbly coast. 2: High rocky coast. 3: Low sandy coast. 4: Low sandy-pebbly coast. 5: Sediment drift. 6: Average direction of the sea wave flux energy. 7: Limit between III order CPUs. 8: Very high risk to coastal erosion (P4). 9: High risk to coastal erosion (P3). Acronyms: CM: Cape Milazzo; CR: Capo Rasocolmo; CP: Cape Peloro; CSR: Cape San Ranieri; CS: Cape Scaletta. The figure was based on data reported in [48].

According to [45], the Cape Peloro's coasts fall into two CPUs (CPU n. 1 and n. 2) [45–48] (Figure 2a).

CPU n. 1 faces in the Tyrrhenian Sea for about 46 km, being stretched from Cape Milazzo (at W) to Cape Peloro (at E) [45–48] (Figure 2a). The main sedimentary supply derives from about ten streams. During the last two centuries, the Tyrrhenian side of Cape Peloro's beaches was carefully examined and stated "to be naturally stable within the same sector, resulting in a change in shape without any loss in volume" [49]. Nonetheless, a significative erosion evaluated in a loss of about 12,000 m^2 of beach occurred in 2012, whereas the Cape Peloro beach underwent an accretion of about 5000 m^2 [49]. An increase in the intensity of the winds from WNW–NW and a decrease in the wind energy blowing from NW to NNE have been observed since 2005 [49].

CPU n. 2 extends for about 50 km along the Messina Straits, from Cape Peloro (at NNE) to Cape Scaletta (at SSW) [45–48] (Figure 2a). The main sedimentary supply derives from about twenty streams. Tide currents in the proximity of Cape Peloro are ENE-wards during the ascending phases and WSW-wards during the descending phases.

According to the recent valuable research carried out for the Sicilian region (project PRCEC [48]), the Sicilian coasts may be subdivided in CPU ranking from I to IV in order. In this modern proposed subdivision, the Cape Peloro coasts would better belong to the III order CPU (n. 10.1.2), denoted Cape Rasocolmo–Cape San Ranieri [48] (Figure 2b), in its turn belonging to a II order CPU (or macro-cell) (n. 10.1), denoted Cape Milazzo–Cape San Ranieri (Figure 2b). In particular, in the Cape Rasocolmo–Cape San Ranieri CPU, the average direction of the sea wave flux energy and the sediment drift are SSE-wards and ESE-wards, respectively, in the Tyrrhenian coast, whereas they are NW-wards and NNE-wards, respectively, in the Ionian coast [48] (Figure 2b). In the CPU Cape Milazzo–Cape San Ranieri, about 14% and 2% of the coasts are affected by a very high (P4) and high risk (P3) to coastal erosion [48]. Six and two localities, P4 and P3, respectively, fall in the CPU Cape Rasocolmo–Cape San Ranieri in the proximity of the study area [48] (Figure 2b).

5. Materials and Methods

During the time lapse November 2023–December 2024, geological surveys, photographic reports, and sampling activities were intensively performed on the foreshore and backshore of the Cape Peloro peninsula, where preliminary data on the finding of ACMs were recently reported [24]. The study materials were beach siliciclastic sediments (sands, pebbles, cobbles) containing significative amounts of technofossils (ACMs, bricks, slabs, tiles, concrete, and glass). Sampling (or observation) activities were carried out to reach an amount (or evidence) representative of all the main lithologies, technofossils, and shapes characterizing the study area. Furthermore, two samples of the Messina Formation (i.e., the sediments underlying the studied beach sands) were also examined, in order to hypothesize the provenance of beach pebbles and cobbles.

Another representative locality, surveyed to better understand the causes of the beach contamination by ACMs, was individuated along the Ionian coast, about 10 km south of Cape Peloro (near the Annunziata stream mouth; Figure 1).

Analyses were devoted to characterizing the petrographic composition and the textural features (grain size distribution, shape, roundness) of these materials. Analyses were performed in the Forensic Geology laboratory of the University of Messina.

Due to the danger of some materials (ACMs), proper personal protective equipment (PPE) was used during the analyses of all the studied specimens.

5.1. Petrographic Analyses

A preliminary visual inspection (VI) was devoted to pebbles, cobbles, and technofossils, in order to characterize their mesoscale petrographic features by means of the human eye. Due to their evident mesoscale compositions, textures, and structures, most of these materials were easily classifiable. The identified features allowed the author to compare the natural samples with the typical main lithotypes diffused in the Peloritani chain and the

technofossils with construction and demolition materials. VMI, optical microscopy (OM), and X Ray powder diffraction (XRD) were carried out on the sands.

Petrographic analyses were performed on thin sections of pebbles and cobbles and on sands aggregated in epoxy resin.

The instruments used for OM were a stereomicroscope (Zeiss, Stereo Discovery model, Oberkochen, Germany) and a petrographic microscope (Axio Vision model, Zeiss, Oberkochen, Germany). Both microscopes were coupled to a telecamera and workstation using image analysis software (Zeiss, model Axiovision, version 4.6, Oberkochen, Germany).

XRD was used for the phase identification of crystalline materials, in order to provide the average bulk mineralogical composition. Sandy samples collected in the study area, after being finely ground in an agate mortar with an agate pestle, were packed in sample holders and scanned by the diffractometer with angles in the range 5–70°. The instrument used was a bench diffractometer (Bruker, model D2 phaser, Billerica, MA, USA). The software for identifying the mineral composition was Diffract EVA (Bruker, Billerica, MA, USA).

Most of the minor minerals, present in the sandy samples as mono- and polymineral lithoclasts, not detectable by means of XRD, were identified under a stereomicroscope by means of OM observations of grain luster, color, habitus, and cleavage, when preserved. In addition, unpublished data on micro-Raman analyses were used to confirm the OM and XRD determinations on heavy minerals.

5.2. Particle Size Analysis (PSA)

PSA was carried out through mechanical sieving for the sands and laser light scattering method for the silts.

5.2.1. Mechanical Sieving

The mechanical sieving of the sands is usually performed in order to separate and weight the different grain sizes for obtaining the particle size distribution in cumulative and frequency curves.

The sands used for the PSA were prepared, pre-treating them with H_2O_2 (for eliminating the organic matter) and drying them in oven at 80 °C. The sieves used to analyze sands had the following sieve openings: −1, 0, 1, 2, 3, 4 phi [−log 2 d(mm)]. Additional sieves were used for the analysis of the sands with minor amounts of gravel (−4.2, −3.6, −3.2, −2.7, −2.2, −2.0 phi). The instrument used was a mechanical siever (Retsch, model AS2, Haan, Germany). After the mechanical sieving, each particle size was weighted and separated in different sample holders.

Statistical parameters, such as the central tendency (mean and median), standard deviation (sorting), skewness, and kurtosis, were calculated using the Folk and Ward method [50]. Parameters were calculated in spreadsheets (Excel 2021 software) and expressed in cumulative and frequency per cent curves.

5.2.2. Laser Light Scattering

The laser diffraction technique is usually used for the PSA of finer particles < 4 phi (62.5 μm). The method of the laser light scattering is based on the concept of the equivalent sphere, i.e., the volume of an irregular particle may be approximate to the volume of a sphere. In the method, the size distribution of particles is obtained by the forward diffraction of a laser beam by the particle. The diffraction angle is inversely proportional to the particle size, whereas the intensity of the diffracted beam may quantify the number of particles [51,52].

The undersize sediments, related to the 4 phi sieve of the sands, were measured by means of a diffraction particle size analyzer in wet conditions. The instrument used was a laser diffraction particle size analyzer (Malvern Panalytical, Malvern, UK, model Mastersizer 2000) able to measure particles in the size range 0.02–2000 μm.

Textural data were automatically calculated by software (Mastersizer 2000) and expressed in cumulative and frequency per cent curves.

5.3. Shape and Roundness

The morphological and morphometric analyses of the sediments were performed to investigate the main shape parameters (flatness, elongation, sphericity, and roundness [53]) of pebbles, cobbles, sands, and technofossils.

The coarse sizes (pebbles, cobbles, and technofossils) were examined, measuring the short axis (S = Short or c), the medium axis (I = Intermediate or b), and the long axis (L = Long or a) of each particle by means of a caliper [53]. For these materials, the flatness (F = I/S) and elongation (E = L/I) ratios were also calculated, in order to classify the 3D shape in the Zingg diagram [53]. The shape parameters were managed in spreadsheets and plotted in box plots (Excel 2021 software) reporting the main statistical data (minimum value Q0; first quartile Q1; median value Q2; third quartile Q3; maximum value Q4; standard deviation).

To be able to compare the same shape parameter in coarse materials and sands, the 2D shape parameter related to the sphericity (Riley sphericity) [53], obtained by measuring the D_i (inscribed diameter) and D_c (circumscribed diameter) of particles, was determined using image analysis software (Axiovision, Zeiss, Oberkochen, Germany) applied on high-resolution photographs taken under a microscope.

The roundness of the sediment particles was determined by using comparative charts [53].

Technofossils' special ornamentations or marks (threads, textures, holes, etc.) were also searched and analyzed under a microscope to better ascribe them to the specific product classes.

6. Results

6.1. Samples

In the foreshore and backshore of the study area, geological surveys allowed the author to recognize several hundreds of inorganic fragments of waste, mostly consisting of construction and demolition materials. These were present mostly in the surface but also within the beach sediments as technofossils. Huge amounts of plastics (bottles, containers, etc.) were also present, but only inorganic waste was the object of the present research.

Due to the significative occurrence of construction and demolition materials, the fragments were randomly observed, identified, recorded by means of photographic acquisition, and counted along a 400 m longshore section parallel to the Tyrrhenian coast. The inspection carried out in December 2023 resulted in about 750 fragments of wastes, among bricks, pottery, tiles, stoneware slabs, cement, glass, and ACMs. Analogous inspection, carried out in the same period in the Ionian side, especially in the Torre Faro village (Figure 3c), indicated an exponential increase in the amounts of these materials, ACMs included.

Ten samples of beach sandy deposits (TB01–10) were collected on the foreshore and backshore (Figure 3b). On the base of the significative amounts of ACMs found during the previous surveys [24], the sand sampling in the sector of the Torre Faro beach was not carried out, to protect the author's safety (Figure 3c). Foreshore samples were collected parallel and orthogonal to the coastline. Samples TB04–05–06 (Figure 3b) were collected along a N–S oriented transect along the Tyrrhenian coast, during a sea storm. The others were mostly collected in the central zone of the beach. One sample (TB08) was collected on the backshore.

Two samples of coarse sediments (TB11–12) and four samples of anthropogenic inorganic wastes (TB13–16) were collected, each one in a collective specimen, along the shoreline of the study area.

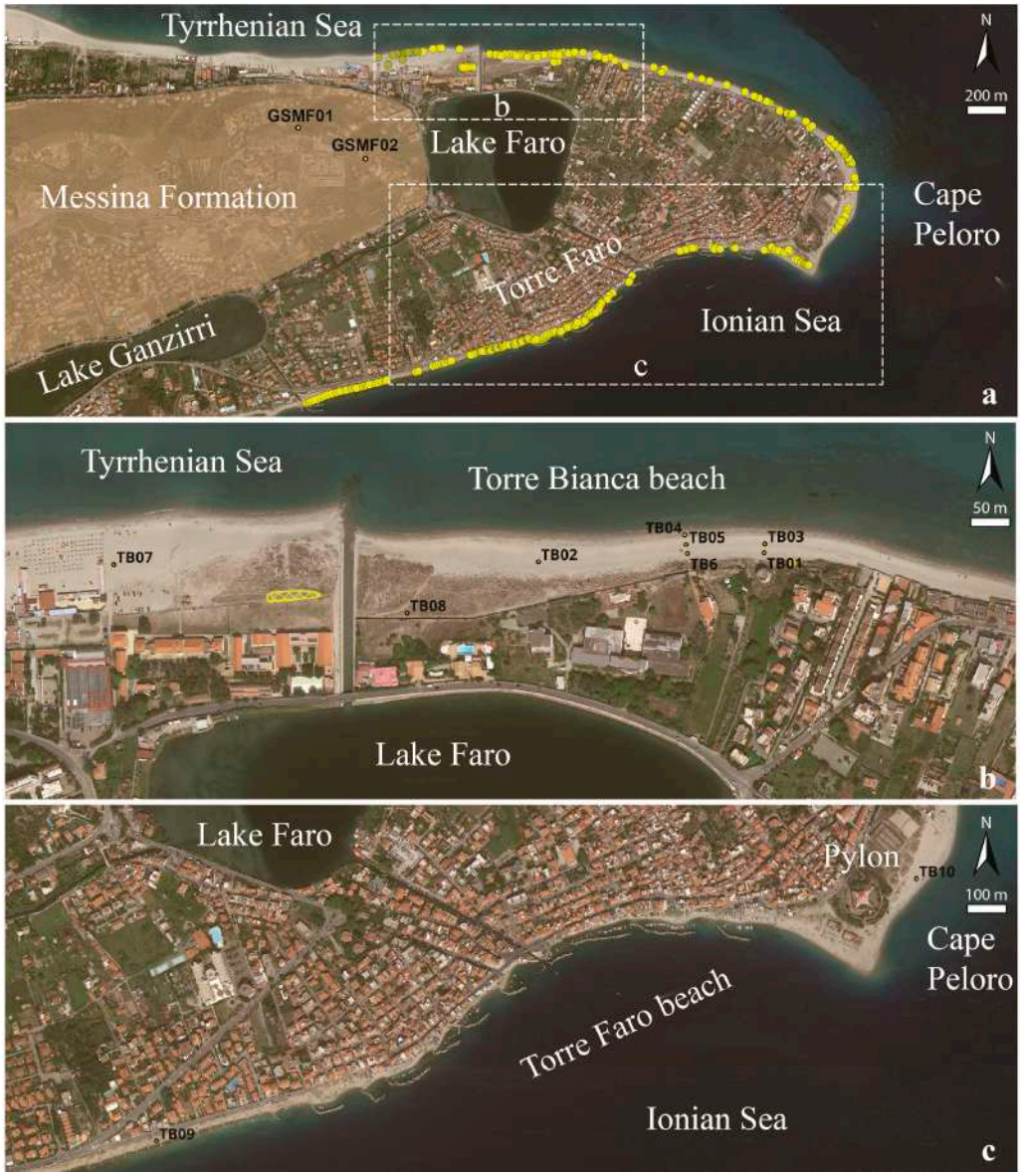

Figure 3. QGIS map of the study area. (**a**) Cape Peloro peninsula—Satellite image showing sites (yellow circles: ACMs inside the reserve; green circles: ACMs outside the reserve) where ACMs were documented by means of high-resolution photographs in [24]. The hills on the western side of Lake Faro are formed by the Quaternary Messina Formation (evidenced in light brown color; samples GSMF01–02). The two rectangles (**b**,**c**) indicate the sampling area for the ten samples of beach sands. (**b**) Torre Bianca beach in the Tyrrhenian coast—Satellite image showing the distribution of the beach sandy samples (TB01–08) and of a superficial landfill of ACMs (area with yellow line and pattern). (**c**) Torre Faro beach in the Ionian coast—Satellite image showing the distribution of the beach sandy samples (TB09–10).

Sample TB11 was made up of pebbles and cobbles composed of high-grade metamorphic rocks (MP), whereas Samples TB12 and TB13 were composed of pebbles and cobbles of porphyroids (PP) and andalusite bearing phyllites (AP), respectively.

The samples of variegated fragments of wastes were as follows:

1. Sample TB14, formed by representative fragments of natural pebbles of anthropogenic origin (NP), originally forming tiles and stoneware slabs.
2. Sample TB15, made up of fragments of colored glass (G).
3. Sample TB16, composed of representative fragments of bricks, tiles, and concrete (PT).

Two additional samples (GSMF01–02) of the sands and gravels of the Quaternary Messina Formation, exposed on the nearest outcrops present in the hills surrounding Cape Peloro (Figures 1 and 3a), were collected for comparative purposes.

6.2. Petrographic Characterization

6.2.1. Beach Sands

VI and OM observations on the beach sands (Samples TB01–10) revealed that the composition of the studied samples was very homogenous. Sands were mainly composed of monomineral siliciclastic grains showing typical features compatible with hyaline quartz (Figure 4a), white feldspars (Figure 4d–f), biotite (Figure 4g), and polycrystalline grains mostly composed of quartz + biotite and quartz + feldspar + biotite paragenesis (lithoclasts of gneiss and granitoids) (Figure 4b,c). Minor glassy grains of light gray to black volcanic particles (Figure 4i) and monocrystalline grains of the group of muscovite (Figure 4h) were also found.

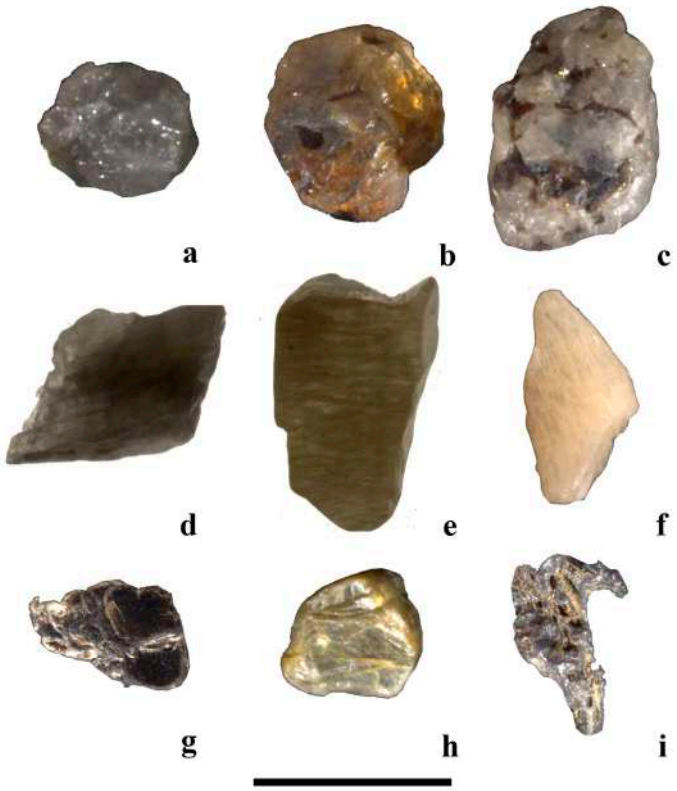

Figure 4. Main types of mineral grains forming the sands (Sample TB01, 1–2 mm sandy fraction), observed under stereomicroscope. (**a**) Quartz. (**b**,**c**) Polymineralic grain of quartz + feldspar + biotite gneiss (**b**) and augen gneiss (**c**). (**d**–**f**) Monomineralic grain of feldspar showing typical cleavage, and pinkish color in (**f**). (**g**) Monomineralic grain of biotite showing typical black color and cleavage. (**h**) Monomineralic grain of muscovite showing typical white color and cleavage. (**i**) Volcanic grain with vesicular texture. Reflected light in (**a**–**c**,**g**–**i**). Transmitted light in (**d**–**f**). Scale bar: 1000 µm.

The 1–2 mm grain size of sands was also examined for the search for minor minerals, such as the heavy minerals. A heavy minerals search by hand picking under a stereomicroscope allowed the author to identify significative amounts of hyaline garnets and, in minor percentages, olivine and other femic minerals. Garnets were found mainly concentrated in the sandy fraction 1–2 mm of one sample collected in Tyrrhenian sands (TB01) and one from the Ionian sands (Sample TB09). Some of the garnets preserved their typical crystalline habitus, hyaline luster with typical red violet to pink color (Figure 5a–f,h–j), and mineral inclusions (Figure 5i). The olivines found were green and all preserved their habitus (Figure 5g).

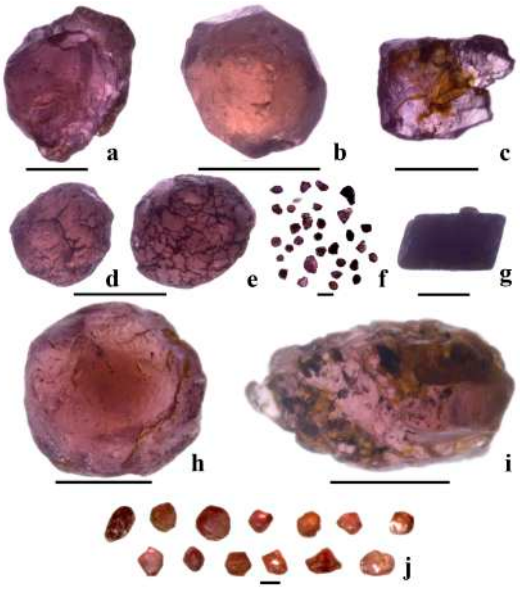

Figure 5. Main types of heavy mineral grains (1–2 mm size) present in the beach sands, observed under stereomicroscope [(transmitted light in (**a**–**i**); reflected light in (**j**)]. Sample TB01: (**a**–**f**) Almandine garnets. (**g**) Olivine Mg end member (namely forsterite). Sample TB09: (**h**–**j**) Almandine garnets. Garnets show traces of presumable Mn dendrites in (**e**) and inclusions of ilmenite in (**i**). Scale bar: 1000 μm.

Modern bioclasts (searched in untreated samples) were scarce and mostly represented by pelagic and benthic foraminifers, gastropods, bivalves, and other fragments of marine organisms.

The technofossils found in the sands were mostly formed of dark and light green (Figure 6a,b) and orange (Figure 6c) glass fragments and concrete. Metal anthropogenic fragments (Figure 6d) were also found. Evidence of fragments of mm-sized pottery and ACMs, found in the coarsest beach materials, was not found in the sands.

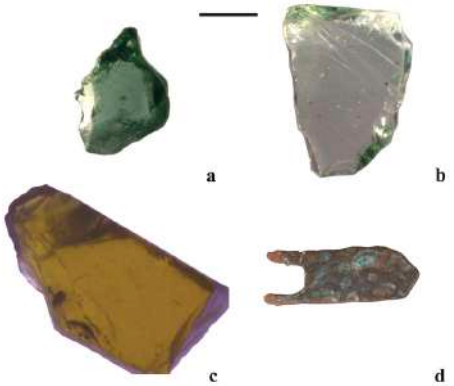

Figure 6. Technofossils present in the sands (Sample TB01, 1–2 mm sandy fraction) observed under stereomicroscope [(transmitted light in (**a**–**c**)]. (**a**) Dark green glass fragment. (**b**) Light green glass fragment. (**c**) Orange glass fragment. (**d**) Metal fragment (reflected light). (**a**,**b**): Scale bar: 1000 μm. (**c**,**d**): Scale bar: 2000 μm.

The thin section analyses of beach sands (Samples TB01–10) under petrographic microscope indicated that sands were quartzo–lithic rich, mostly being formed of monomineral grains of quartz (50–60%) (Figure 7a–c) with minor plagioclase, k-feldspar (Figure 7d,e), opaque minerals (Figure 7f), and almandine garnet grains (Figure 7g–i), and metamorphic lithics (40–50%), mainly composed of polymineral quartz + microcline, quartz + plagioclase, quartz + biotite, and quartz + muscovite grains (Figure 7j–o).

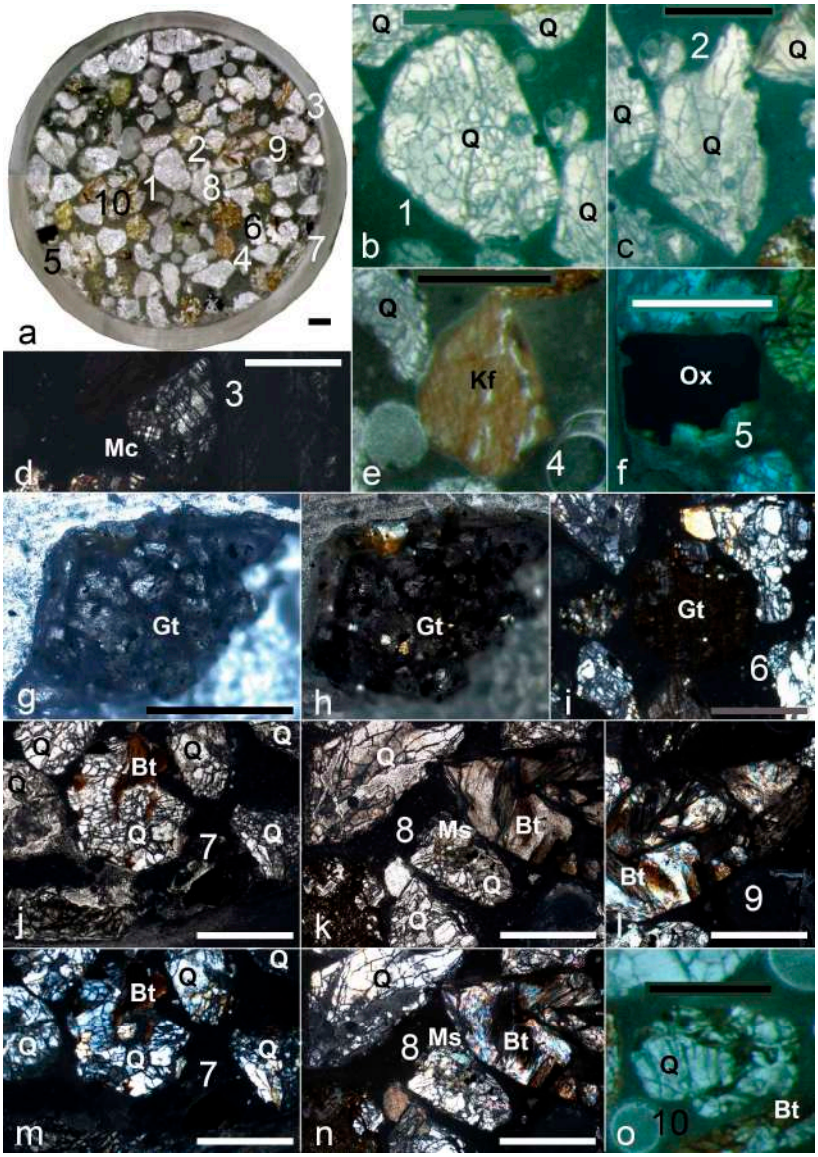

Figure 7. Petrofacies of modern sands (aggregated in epoxy resin), mainly composed of grains of quartz and lithoclasts (Samples TB05 and TB09). (**a**) Thin section (observed in transmitted light under stereomicroscope; numbers indicate the grains reported in (**b**–**f**,**i**–**o**); Sample TB09). (**b**) Very fractured sub-rounded quartz grain (observed in transmitted light under stereomicroscope). (**c**) Very fractured angular quartz grain (observed in transmitted light under stereomicroscope). (**d**) Rounded polymineral lithoclast composed of quartz + microcline (observed under microscope, XPL). (**e**) Sub-rounded monomineral grain composed of k-feldspar showing cleavage (observed in transmitted light under stereomicroscope). (**f**) Sub-rounded monomineral grain composed of opaque mineral (observed in transmitted light under stereomicroscope). (**g**–**i**) Grains of almandine garnet. (**g**) Angular grain of almandine (observed under microscope, PPL; Sample TB05). (**h**,**i**) Grain of almandine preserving euhedral habitus (observed under microscope, XPL; Sample TB09). (**j**–**n**) Polymineral lithoclast composed of quartz + biotite and quartz + muscovite (observed under microscope, PPL (**j**), XPL (**m**); Sample TB09). (**k**–**n**) Polymineral lithoclast composed of quartz + muscovite + plagioclase + opaque (observed under microscope, PPL, Sample TB09. (**k**), XPL (**n**). (**l**) Well-rounded polymineral lithoclast composed of quartz + biotite + muscovite (observed under microscope, XPL). (**o**) Sub-rounded polymineral lithoclast composed of quartz + biotite + opaque (observed in transmitted light under stereomicroscope e). Acronyms. Q: Quartz. Kf: k-feldspar. Mc: Microcline. Ox: opaque minerals. Gt: Garnet. Bt: Biotite. Ms: Muscovite. PPL: plane polarized light. XPL: crossed polarized light. Scale bar: 1000 μm.

Peculiar microstructures were distinguished in the quartz and garnets. The quartz grains were pervasively fractured along different joint systems (Figure 7b,c). The garnets showed quartz trails and relics of crenulation cleavage (Figure 7i).

Due to the homogenous composition of the samples ascertained on tens of thin sections, XRD analyses were carried out in only one sample (TB02). Analyses were performed on the bulk powder of the sand as it was and on the undersize fraction to the sieve 4 phi (62.5 μm). The mineral composition of the sands was mainly characterized by quartz + biotite + muscovite + albite, confirming the petrographic observation under microscope.

The mineral composition of the undersize fraction to the sieve 4 phi (62.5 μm, Sample TB02) was similar to that of the sands, being characterized by quartz + biotite + albite. Anorthite was also found. Presumably, the muscovite present in the sand sample was not revealed in the finest fraction because its amount was under the reliability limit of the instrument.

6.2.2. Pebbles and Cobbles

The representative modern beach pebbles and cobbles (Sample TB11) were mainly composed of acid intrusive and metamorphic rocks, the latter affected by high-grade metamorphism.

Indeed, the composition was mostly represented, in order of abundance, by the following:

1. Gneiss and micaschist gneiss (Figure 8a).
2. Augen gneiss (Figure 8b).
3. Biotite-bearing granitoids (Figure 8c).
4. Quartz (Figure 8d) and quartz with biotite.

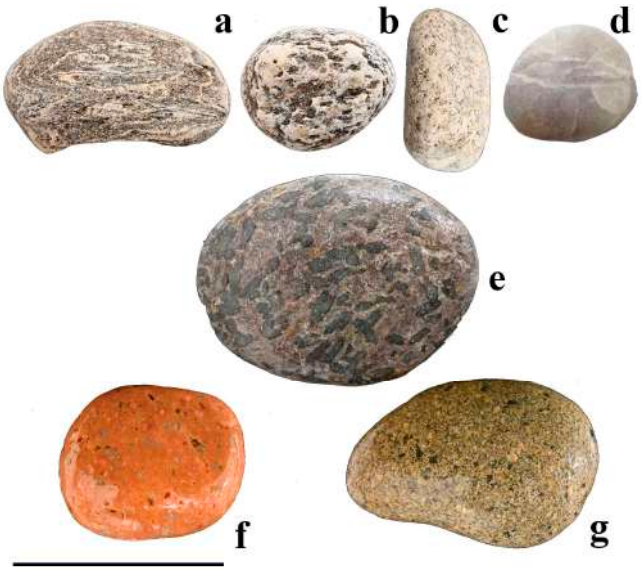

Figure 8. Typical aspect and composition of the main pebbles and cobbles forming the beach deposits. (**a**) Gneiss (Sample TB11). (**b**) Augen gneiss (Sample TB11). (**c**) Granitoid (Sample TB11). (**d**) Quartz (Sample TB11). (**e**) Dark grayish sericitic phyllite with randomly oriented post-kinematic andalusite porphyroblasts (Sample TB13). (**f**) Pinkish porphyroid clast (antique pink type color, Sample TB12). (**g**) Light grayish porphyroid clast (Sample TB12). Scale bar: 5 cm.

Notwithstanding being present in minor amount, the typical pebbles and cobbles characterizing the studied modern beach deposits were composed of low-grade metamorphic rocks and magmatic rocks. These consisted of the following:

1. Andalusite bearing sericitic phyllites (Sample TB13, Figure 8e).
2. Pinkish or grayish porphyroids (Sample TB12, Figure 8f,g).

Light gray and blackish pumice rock fragments of Eolian provenance were also found in the studied area.

Very few pebbles of whitish to beige vacuolar limestones (Messinian) and coral rudstones (lower Pleistocene) were also detected.

6.2.3. Technofossils

Construction Slabs

OM observations on the coarse anthropogenic construction and demolition material (Sample TB014) allowed the author to identify fragments of construction slabs made up of sedimentary, magmatic (volcanic and intrusive), and metamorphic rocks. They were, in order of abundance, as follows:

1. Limestones (Figure 9(1–13,14–23,26)) and arenites (Figure 9(24,25)).
2. Magmatic rocks (Figure 9(27–35)).
3. Marbles (Figure 9(14)).

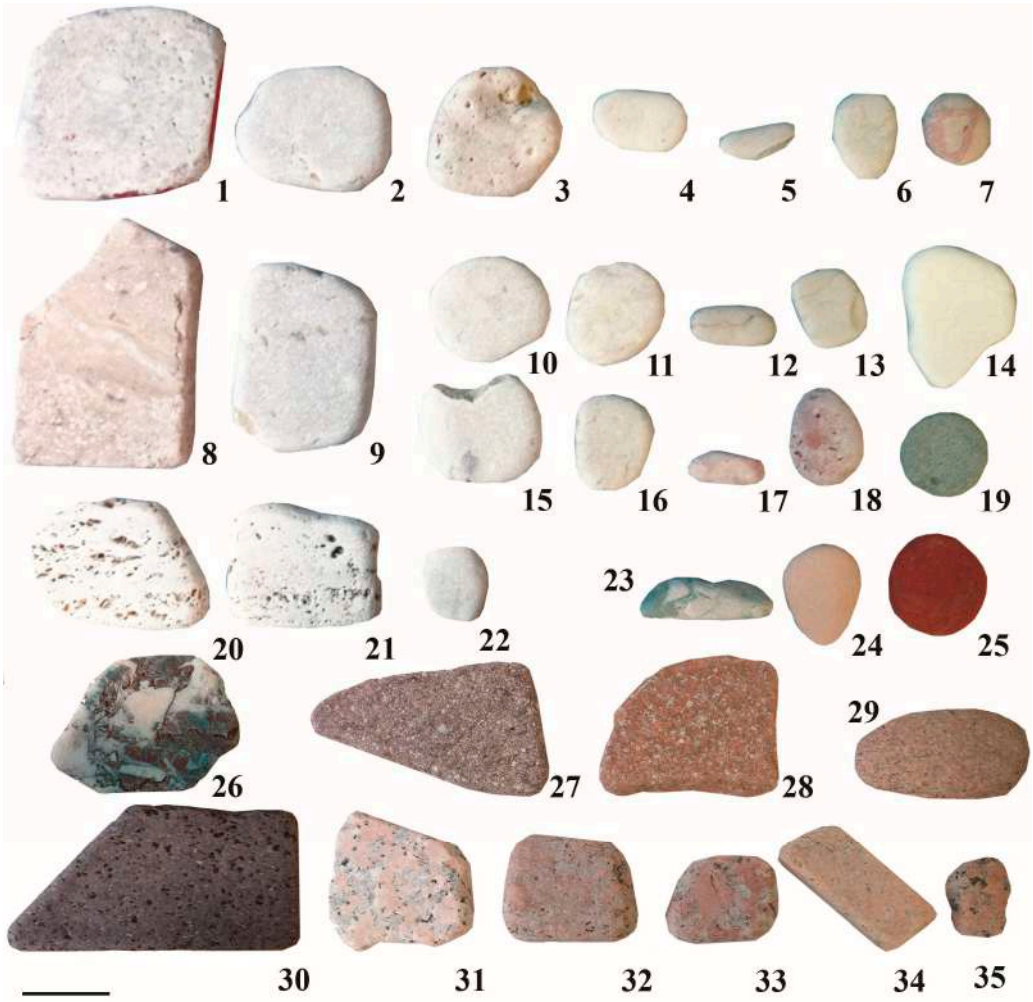

Figure 9. Technofossils—Construction slabs (Sample TB14). (**1**–**13**,**15**–**19**,**22**,**23**,**26**) Sedimentary calcareous rocks (grainstones, packstones, wackestone, mudstones). (**20**,**21**) Travertines. (**24**,**25**) Arenites. (**14**) Metamorphic rocks: Marble. (**27**–**29**) Volcanic rocks: Porphyroids. (**30**) Basalt. (**31**–**35**) Intrusive rocks. Granite (**31**). Feldspar granite (**32**–**35**). Scale bar: 5 cm.

Anthropogenic Glass

OM observations on the coarse fragments of anthropogenic glass (TB015, Figure 10) collected in the beach deposits allowed the author to distinguish the following colors, in order of abundance: green (dark to light green bottle), white, and orangish–brownish (Figure 10).

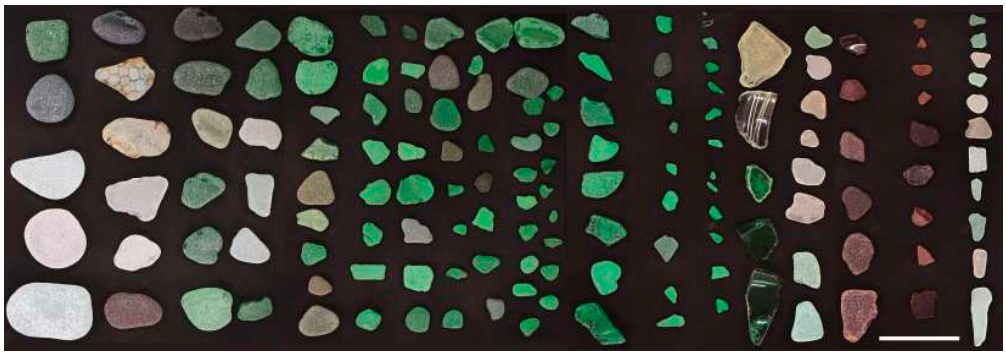

Figure 10. Technofossils—Glass (Sample TB15). Green (green bottle), white, orangish–brownish, and transparent fragments of glass. Scale bar: 5 cm.

Bricks, Tiles, Concrete

OM observations on the demolition and construction materials present in the beach deposits allowed the author to distinguish the fragments mostly represented, in order of abundance, by bricks, tiles, and concrete (TB016, Figure 11). Huge amounts of bricks and tiles were evident in the beach of Torre Faro.

Figure 11. Technofossils—Bricks, tiles, concrete (Sample TB16). Clay-made materials mostly composed of orangish–brownish bricks consisting of perforated or solid types and roof tiles. Black burn fragments of construction material (on the left). Tiles, mostly glazed tiles, showing characteristic colors and designs typical of the 1970s–1980s' building materials. Scale bar: 5 cm.

ACM

Special attention was devoted to characterizing the aspect of the ACM. It was mainly characterized by corrugated shapes (Figure 12a–f) showing typical honeycomb ornamentations (Figure 12a) or with remnants of incapsulating paints. The identification of fibers with features compatible with asbestos minerals, such as crocidolite and chrysotile fibers [24], allowed the author to classify fiber cement as ACM (Figure 12d–f). A minor part of the ACM showed stratified encrustations of marine organisms, such as algae, Bryozoa, and Vermetids (Figure 12g) grown on previous lichens. The beach of Torre Faro showed huge amounts of waste, mostly composed of concrete, bricks, and tails with ACMs (Figure 12h,i).

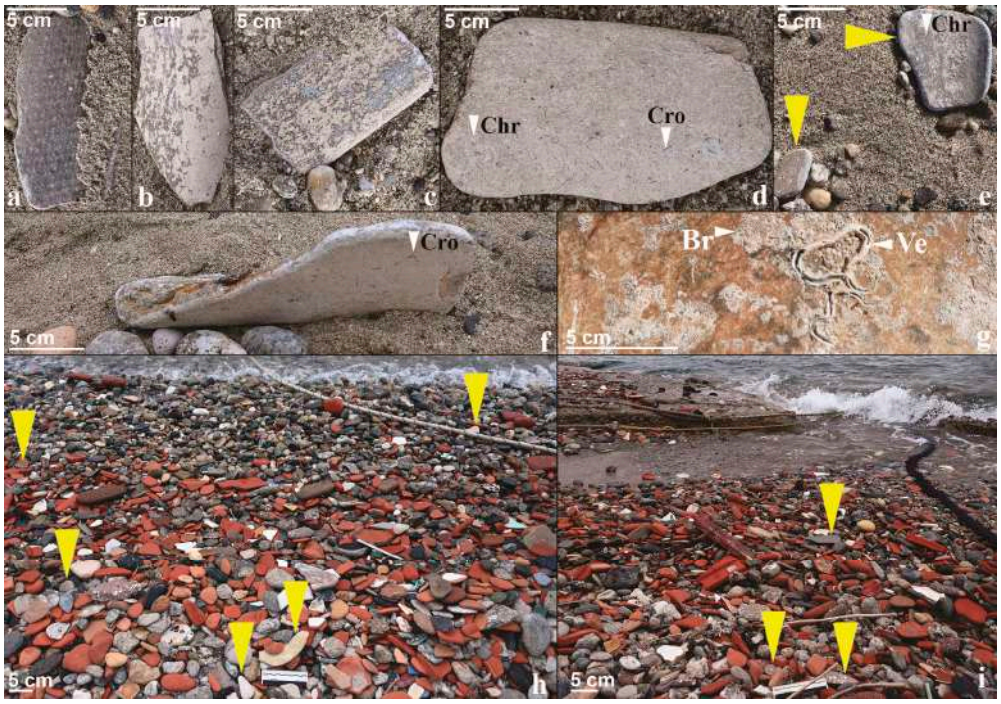

Figure 12. Technofossils present in the Cape Peloro beaches. (**a**) Fragment of ACM showing honeycomb texture and rounded shape. (**b**) Angular fragment of ACM. (**c**) Sub-angular fragment of ACM. (**c**–**f**) Fibers of crocidolite (Cro) and chrysotile (Chr) are evident on the ACM fragments. (**g**) Evidence of Bryozoa (Br) and Vermetids (Ve) on ACMs. (**h**,**i**) Anthropogenic deposit made up of concrete, bricks, tails, and ACM, at the Torre Faro beach. Yellow triangles mark ACMs.

6.2.4. Messina Formation

OM investigations on the sample (GSMF01) of gravels of the Messina Formation (Figure 2a) allowed the author to observe pebbles and cobbles dispersed in a sandy matrix. Minor gravel horizons (GSMF02, Figure 2a), weakly cemented by carbonates, showed analogous compositions but different textures, being clast-supported with minor sands in the voids. The particles were mainly formed of acid intrusive rocks and high-grade metamorphic rocks. They consisted of the following:

1. Biotite-bearing granitoids.
2. Augen gneiss.
3. Quartz and quartz with biotite.
4. Gneiss and micaschist gneiss.

Notwithstanding present in minor quantity, typical pebbles and cobbles characterizing the studied Messina Formation deposits were composed of pinkish or grayish porphyroids, analogous to those found in the studied modern beaches.

6.3. Textural Characterization

PSA, VI, OM, and image analysis software were carried out in the modern beach deposits and in the Messina Formation, in order to define the grain size, shape parameters, and statistical data. The shape parameters, elongation (E = I/L) and flatness (F = I/S), being related to the 3D dimensions (LIS), were analyzed only in the coarser rocks (Samples TB12–14) and technofossils (Samples TB15–17) collected on the studied beaches. Riley sphericity and roundness were defined in all the samples.

6.3.1. PSA Data Related to Mechanical Sieving

Ten samples of sandy beach deposits (TB01–10) and one sample of gravels and sands of the Messina Formation (GSMF01) were sieved, by means of mechanical sieving.

The analyses were performed for defining the cumulative and frequency curves of the sediments and the related statistical parameters (mean, median, sorting, skewness, kurtosis).

The foreshore sandy beach deposits were mostly variable between sands (Samples TB01, TB05–06, TB09–10) and weakly gravelly sands (Samples TB02–TB04, TB07). The backshore sample (TB08) was a gravelly sand (Figure 13).

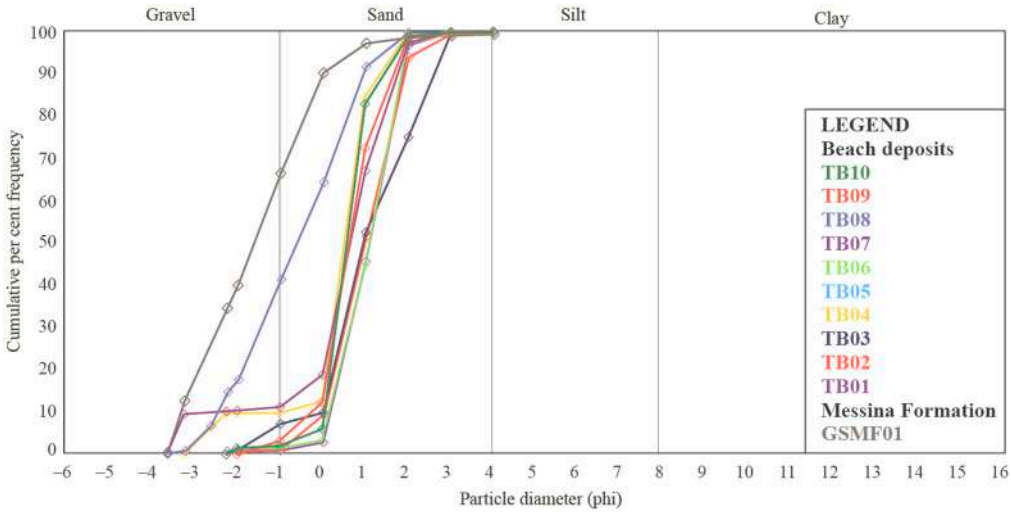

Figure 13. PSA of Samples TB01–10 and GSMF01, expressed by means of cumulative per cent frequencies. Sieves used were spaced from −4 phi (16 mm) to 4 phi (62.5 μm).

The grain distribution was unimodal in 30% of the samples (TB01–2, TB09; Figure 14a), bimodal in 40% of the samples (TB04, TB06–07, TB10), and polymodal in 30% of the samples (TB03, TB05, TB08) (Figure 14b). A maximum of four modes characterized Sample TB08 (Figure 14b).

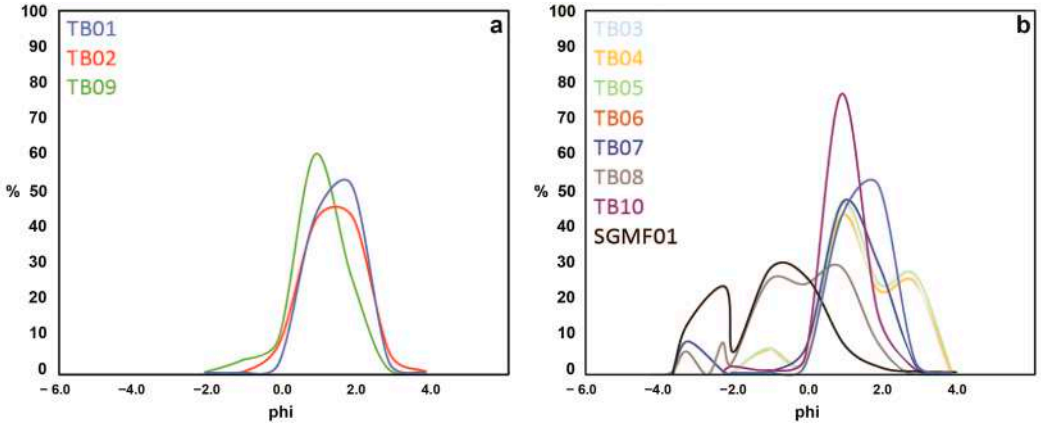

Figure 14. PSA expressed by means of frequency curves. (**a**) Unimodal curves. (**b**) Polymodal curves. Sieves used were spaced from −4 phi (16 mm) to 4 phi (62.5 μm).

The sand mean values ranged from medium to coarse in the foreshore to very coarse in the backshore (Table 1). The median values were mostly comparable with the means, except a few values indicating weakly finer grain sizes (Table 1).

Sorting, ranging from 0.50 to 1.30, indicated that samples were from moderately well (TB10) to moderately sorted (TB01–07, TB09) in the foreshore. Differently, Sample TB08 collected in the backshore was poorly sorted (1.4 phi).

The scatter plot of mean versus sorting of the collected beach sands (TB01–10) showed a decreasing tendency (square-correlation coefficient = 0.2312), where decreasing values of sorting were associated with decreasing grain size (Figure 15), as usually occurs.

Table 1. Statistical parameters (expressed in phi, except skewness) of the oversize fraction to the sieve 4 phi (62.5 μm) beach sandy samples. For the sample locations, see Figure 3.

Parameter	TB01	TB02	TB03	TB04	TB5	TB06	TB07	TB08	TB09	TB10
Mean	1.0	1.0	1.2	0.5	0.6	1.1	0.7	−0.7	0.8	0.6
Median	1.0	1.0	1.0	0.5	0.6	1.1	0.7	−0.6	0.6	0.6
Sorting	0.8	0.8	1.1	0.9	0.6	0.7	1.3	1.4	0.8	0.5
Skewness	−0.1	−0.1	0.2	−0.3	−0.1	−0.1	−0.3	−0.1	0.1	0.0
Kurtosis	0.9	0.8	0.8	2.8	1.9	0.7	1.9	0.8	1.3	1.3

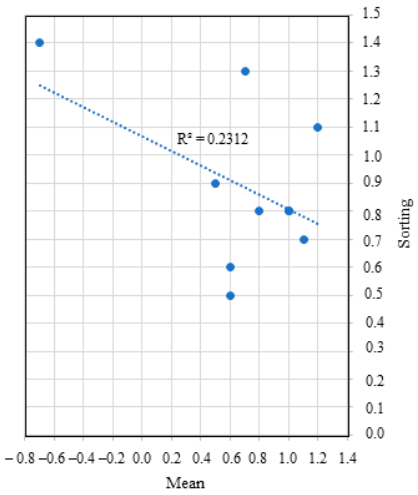

Figure 15. Scatter plot of mean (phi) versus sorting (phi) of the collected beach sands (samples TB01–10). The blue dots and the dashed line represent the samples and the trendline, respectively.

6.3.2. PSA Data Related to Laser Diffraction Method

The PSA of the undersize fraction to the sieve 4 phi (62.5 μm) was carried out in two sandy samples, collected on the Tyrrhenian (Sample TB05) and Ionian beaches (Sample TB09), and in one sample collected in the sands and gravels of the Messina Formation (Sample SGMF01) (Figure 3).

Both undersize fractions of the beach sands, light gray in color (Munsell 10YR 7/1), were composed of coarse silts. The frequency curves were moderately sorted, fine skewed, and leptokurtic (Figure 16 and Table 2).

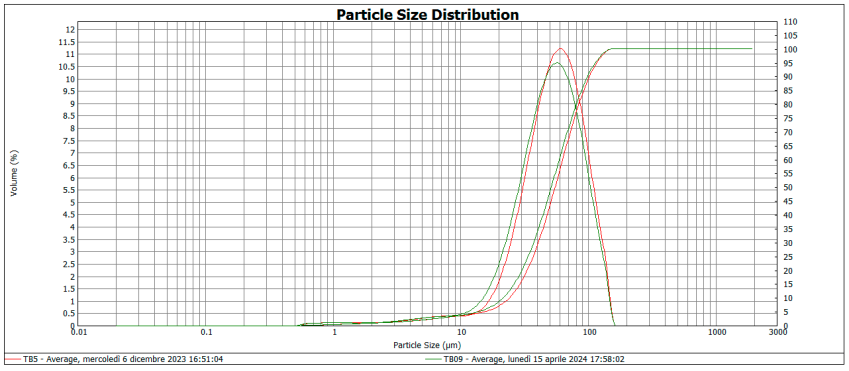

Figure 16. PSA of the beach undersize fraction to the sieve 4 phi (62.5 μm) of Samples TB05 (Tyrrhenian Sea) and TB09 (Ionian Sea). See Table 2.

The undersize fraction of the Messina Formation sample was coarse silts. The frequency curve was poorly sorted, fine skewed, and leptokurtic (Figure 17).

Table 2. Statistical parameters (expressed in phi, except skewness) of the undersize fraction to the sieve 4 phi (62.5 μm) of the samples collected in the beach sands and the Messina Formation. For the sample locations, see Figure 3.

Parameter	TB05	TB09	SGMF01
Mean	4.3	4.3	4.5
Median	4.2	4.3	4.4
Sorting	0.8	0.9	1.1
Skewness	0.2	0.2	0.3
Kurtosis	1.1	1.1	1.3

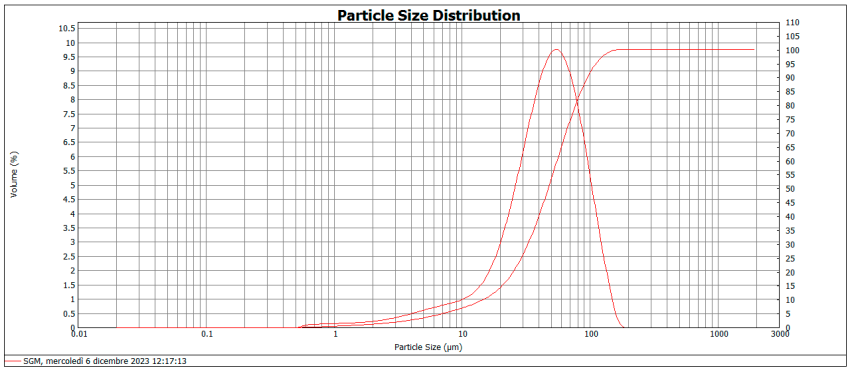

Figure 17. PSA of the undersize fraction to the sieve 4 phi (62.5 μm) of the Messina Formation (Sample SGMF01). See Table 2.

6.3.3. Elongation (E)

The E average values were the highest in the lithoclasts of the beach foreshore deposits, ranging from 0.76 in the NP to 0.81 in the PP, and lowest in the beach foreshore technofossils, ranging from 0.66 in the ACM to 0.72 in the G (Figure 18).

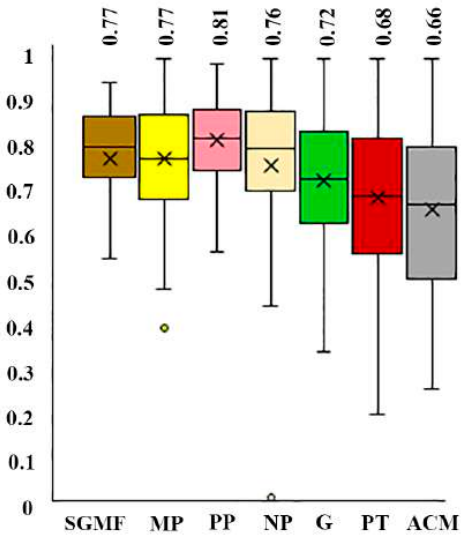

Figure 18. E values of lithoclasts and technofossils selected by the beach deposits. E was also determined in the lithoclasts of the Messina Formation. Mean values corresponding to each cross are reported in the upper part of the graph. Measures were made on 654 elements. Legend. E: Elongation; Lithoclasts—SGMF: Sands and gravels of the Messina Formation (Sample SGMF02); MP: Beach pebbles composed of high-grade crystalline rocks; PP: Beach pebbles composed of porphyroids. Beach technofossils—NP: Natural pebbles of anthropogenic origin; G: Fragments of glass; PT: Fragments of pottery, cement, and tiles; ACM: Fragments of asbestos cement material (E values on ACM are after [23]). Dots represent single values.

The E average values calculated in the sample of gravels from the Messina Formation (SGMF02) were similar to those found in the MP.

6.3.4. Flatness (F)

Analogously, the F average values resulted in the beach foreshore deposits being the highest in the lithoclasts, ranging from 0.51 in the MP to 0.66 in the PP, and lowest in the technofossils, ranging from 0.10 in the ACM to 0.36 in G (Figure 19). The F average values calculated in the sample of gravels from the Messina Formation (SGMF02) were high and similar to those found in the PP.

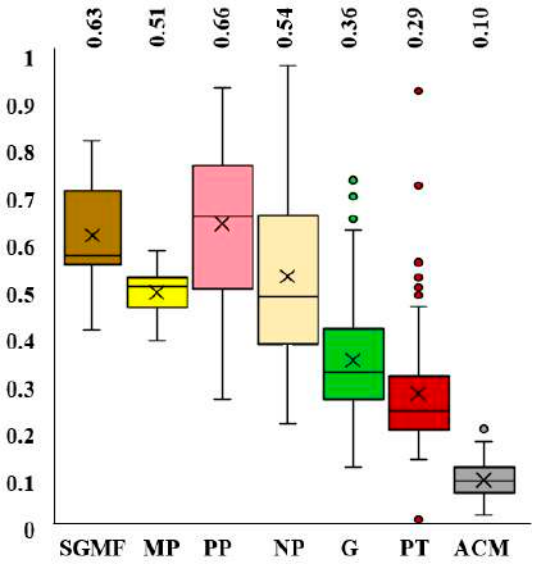

Figure 19. F values of lithoclasts and technofossils selected by the beach deposits. F was also determined in the lithoclasts of the Messina Formation. Mean values corresponding to each cross are reported in the upper part of the graph. Measures were made on 654 elements. Legend. F: Flatness; Lithoclasts—SGMF: Sands and gravels of the Messina Formation (Sample SGMF02); MP: Beach pebbles composed of high-grade crystalline rocks; PP: Beach pebbles composed of porphyroids. Beach technofossils—NP: Natural pebbles of anthropogenic origin; G: Fragments of glass; PT: Fragments of pottery, cement, and tiles; ACM: Fragments of asbestos cement material (F values on ACM are after [23]). Dots represent single values.

6.3.5. Zingg Diagram

The E and F values were useful for defining the main shapes of the beach foreshore lithoclasts and technofossils, plotting these in the Zingg diagram (Figure 20). The shapes of the MP were mostly oblate with minor amounts of equant, prolate, and bladed shapes. The main shapes of the PP appeared oblate and equant with a minor percentage of prolate shapes. The shapes related to NP were mostly oblate with a minor percentage of bladed shapes. The main shapes characterizing the G, PT, and ACM were oblate and bladed. ACM was the flattest material showing the lowest flatness values among technofossils (Figure 20). The main shapes related to SGMF were from prolate to equant (Figure 20).

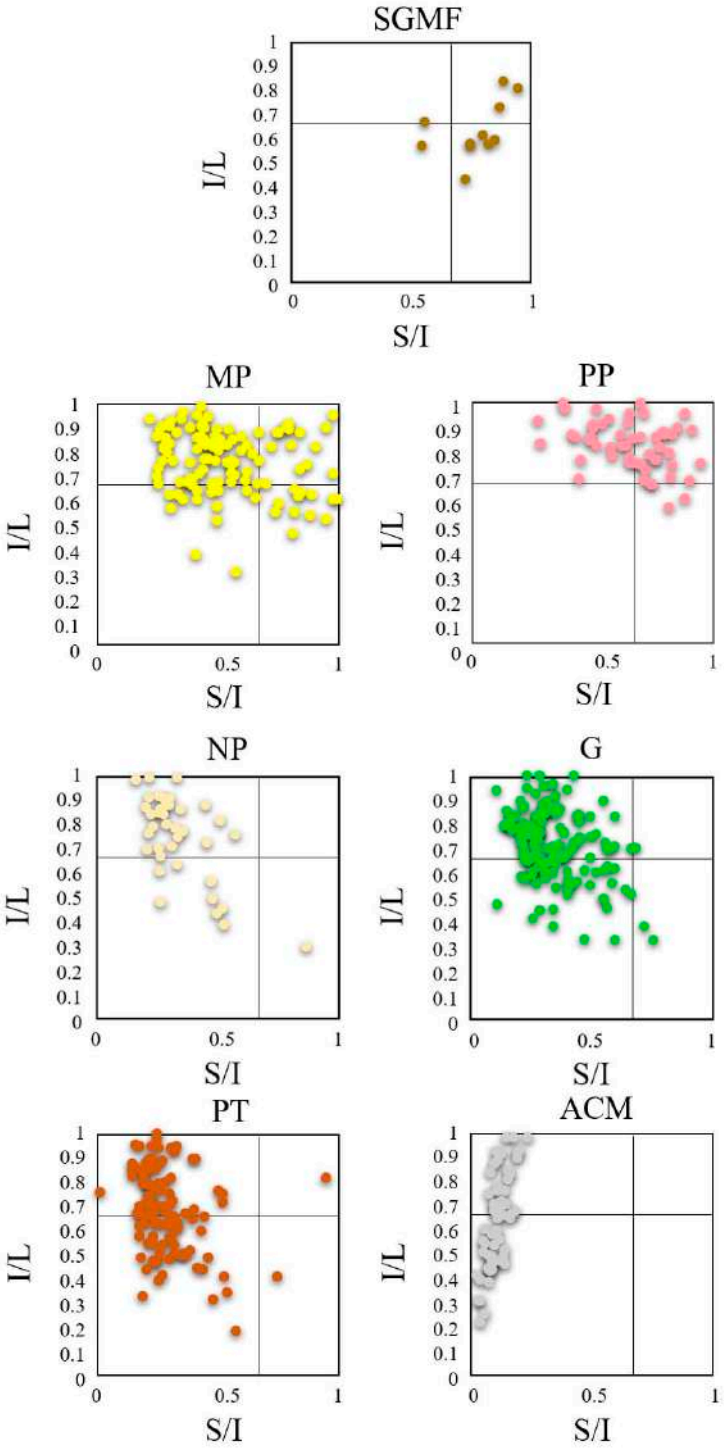

Figure 20. Zingg diagram showing shapes in 3D. S = thickness, I = width, L = length; S/I is the flatness parameter (F); I/L is the elongation parameter (E). Measures were made on 654 elements. Legend—SGMF: Sands and gravels of the Messina Formation (Sample SGMF01); MP: Beach pebbles composed of high-grade crystalline rocks; PP: Beach pebbles composed of porphyroids. Beach technofossils. NP: Beach natural pebbles of anthropogenic origin; G: Beach fragments of glass; PT: Beach fragments of pottery and tiles; ACM: Beach fragments of asbestos cement (E and F values on ACM are after [23]).

6.3.6. Riley Sphericity

The average values of the Riley sphericity analyzed in pebbles and cobbles were highest in the beach lithoclasts (>0.79–0.81) compared to the technofossils (<0.79–0.81) (Figure 21). Indeed, lithoclasts showed sphericity values ranging from 0.83 in the MP to

0.87 in the PP, whereas technofossils presented values ranging from 0.74 in the ACMs to 0.81 in the NP. The Riley sphericity was 0.80–0.82 in the sands. The Riley sphericity average values calculated in the sample of gravels from the Messina Formation (SGMF02) were similar to those found in the PP of the beach deposits.

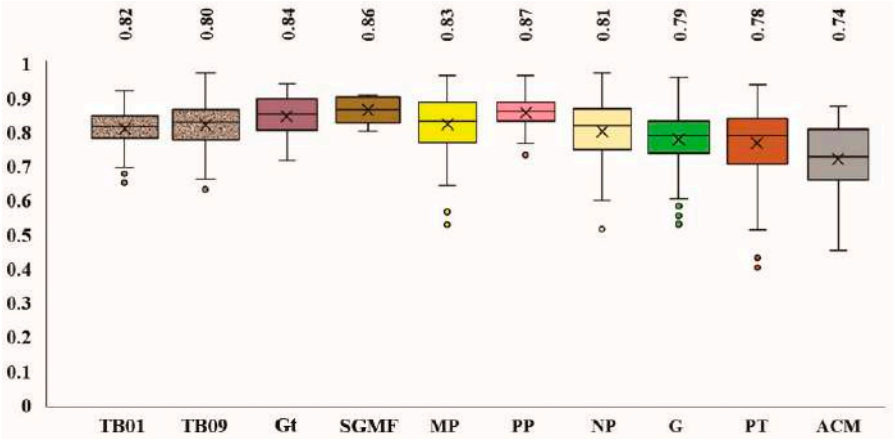

Figure 21. Riley sphericity. Mean values corresponding to each cross are reported in the upper part of the graph. Measures were made on 886 elements. Legend. Lithoclasts—TB01, TB09: Beach sand samples. Gt: Garnets (Sample TB01). SGMF: Sands and Gravels of the Messina Formation (Sample SGMF02); MP: Beach pebbles composed of high-grade crystalline rocks; PP: Beach pebbles composed of porphyroids. Beach technofossils—NP: Natural pebbles of anthropogenic origin; G: Fragments of glass; PT: Fragments of pottery, cement, and tiles; ACM: Fragments of asbestos cement material. Dots represent single values.

6.3.7. Roundness

The roundness of the beach sands, measured on 210 grains, was from angular to sub-rounded (Figure 22). Quartz and feldspar grains were mostly from angular to sub-rounded, and sub-angular, respectively. Metamorphic lithics were mostly sub-rounded (gneiss), and from angular to sub-rounded (phyllites). Among the heavy minerals found, most of the garnets preserved the habitus. Some grains appeared from well-rounded to angular.

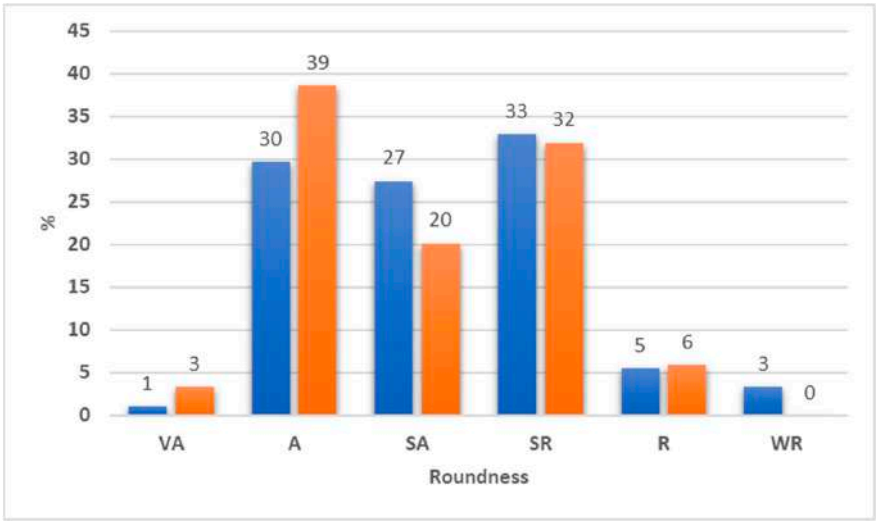

Figure 22. Roundness of sand grains (TB01: blue histograms; TB09: orange histograms). Acronyms. VA: Very angular; A: Angular. SA: Sub-angular. SR: Sub-rounded. R: Rounded. WR. Well-rounded.

The roundness of the beach pebbles and cobbles as well as those of the Messina Formation were mostly rounded.

Technofossils, mostly construction rocks, bricks, and tiles, appeared mostly well-rounded. The glass was mostly well-rounded and in part angular or broken.

The ACMs found in the beach were mostly well-rounded. Angular fragments of ACM were found in an illegal micro landfill intercepted on the backshore and in the winter berms interfering with landfills of demolition wastes individuated near a public resort in front of the Ionian coast in Torre Faro [24]. Analogously, angular fragments were found in the winter berms interfering with landfills of demolition wastes, out of the reserve in the Ionian coast, near the mouth of the Annunziata stream, at Parco Sabin (Figure 23).

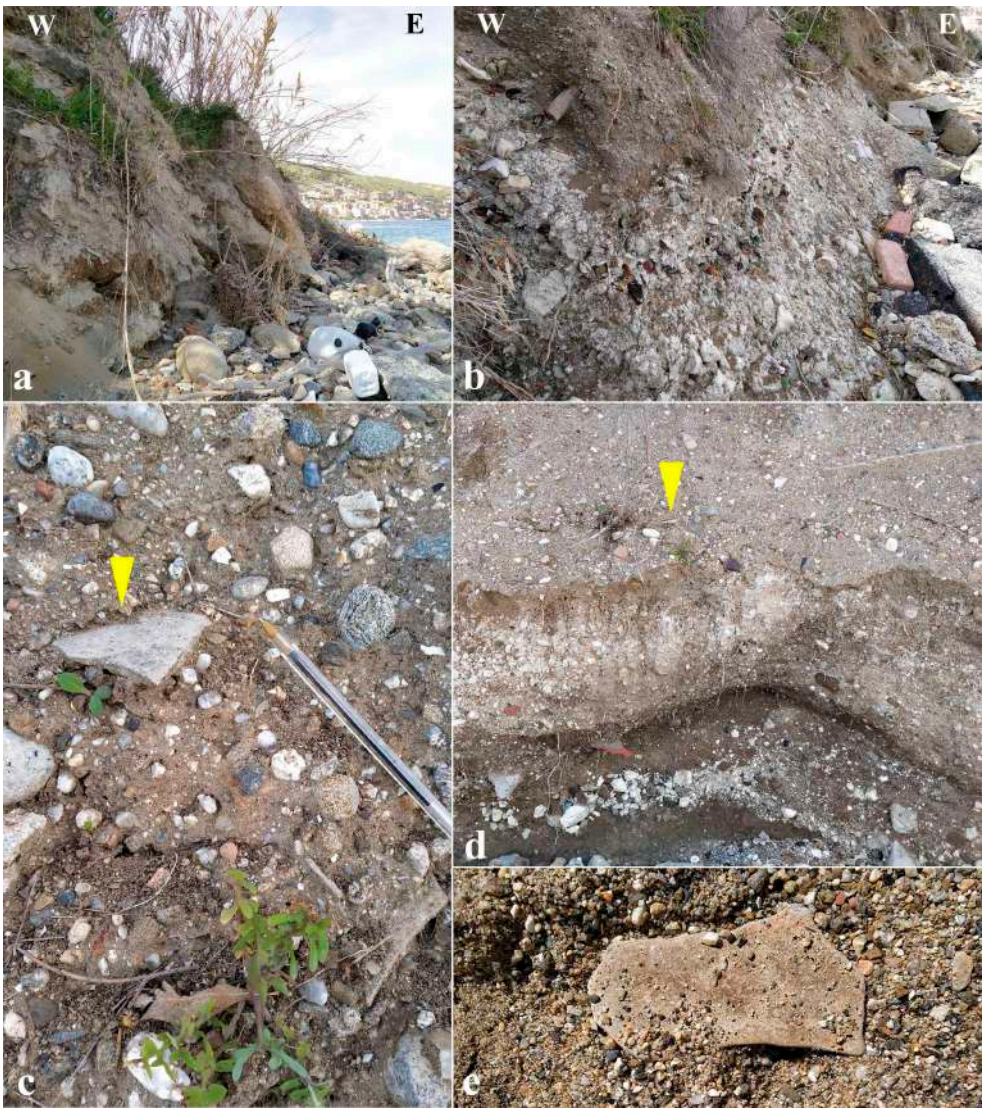

Figure 23. (**a**,**b**) View of the Ionian Sea-wards facing slope of the landfill with construction and demolition wastes present south of the mouth of the Annunziata stream, at Parco Sabin. (**c**,**d**) Angular fragment of ACM. (**e**) Sub-angular fragment of ACM in the alluvial deposits at the Annunziata mouth stream. The yellow triangle marks ACM. See Figure 1 for the localization of the Annunziata stream.

7. Discussion

7.1. Petrographic Features

There are few published data on the petrographic and textural characterization of the Messina modern beach deposits. Cape Peloro's beach sand petrofacies were quartzo–lithic sands, being mainly composed of metamorphic grains of quartz (50–60%), monomineral opaque, plagioclase, k-feldspar, and almandine garnet grains, and metamorphic lithics (40–50%, mainly composed of polymineral quartz + microcline, quartz + plagioclase,

quartz + biotite, quartz + muscovite grains) (Figures 4, 5 and 7). These minerals were mostly the same as those identified by means of XRD in the modern silts collected in the Messina Strait sea floor [54] (area stretched from the Cape San Ranieri to Cape Scaletta). Notwithstanding, the mineral percentages in the study sands were very different, presumably because of the different grain size. Indeed, the sea floor finest deposits were mostly mica-rich.

The modern beach deposits were largely monocyclic, reflecting detritus mostly deriving from crystalline (igneous and metamorphic) basements. These results were consistent with the geological features of the areas including the hydrographic basins facing the CPU "Cape Rasocolmo–Cape San Ranieri" recently reported in the PRCEC project [48], where the beach deposits fall down (Figure 2b). Indeed, the present results together with preliminary data on heavy minerals (Figure 5) should suggest a provenance for the beach mobile sediments, from orogenic sources with high- to medium-grade metamorphic rocks. In particular, the beach sand grains of almandine garnets preserving relics of cleavage systems could originate from the Aspromonte Unit still widely exposed in the northern edge of the Peloritani Mountains (Figure 1).

Differently, the coarsest materials (pebbles and cobbles, Figure 8) of the beach deposits could derive from the cannibalization of the underlying lower to middle Pleistocene SGMF (Figure 3). Indeed, clasts of pinkish and grayish porphyroids (Figure 8f,g) present in the beach deposits are similar to those of the SGMF, widely exposed in the surrounding areas. The origin of the beach pebbles and cobbles from the underlying layers is a common phenomenon usually observed. Differently, the gneiss, augen gneiss, and granitoids forming the beach pebbles and cobbles, being present in both the crystalline rocks of the Aspromonte Unit and in the clasts of the SGMF, could originate from both of them.

Notwithstanding, an open issue persists for the pebbles of sericitic phyllites rich in post-kinematic andalusite (Figure 8e) found in Cape Peloro, because a possible source is actually unknown to the author in the basements of the Peloritani Mountains. These rocks could belong to the highest layers of the Aspromonte Unit of the Calabria–Peloritani Arc or to the lowest basement of the Stilo Unit exposed in Calabria (pers. comm. of Agustin Martin–Algarra). It may be of interest that similar rocks are typical Variscan metamorphites belonging to the Benamocarra Unit in the Betic Cordillera (Spain) [55]. The source areas could be different and complex to identify, because the studied metamorphic lithics could be also cannibalized clasts deriving from different Miocene to Pleistocene siliciclastic sequences of the Calabria–Peloritani Arc.

7.2. Textural Features

7.2.1. PSA Data

The PSA and statistical parameters of the studied modern beach sands, analyzed during winter 2023–2024, indicate that they mainly consisted of moderately to moderately well-sorted (Table 1) sands and gravelly sands, with medium to coarse particles. Analogously, also the silty contents of the sands were moderately sorted (Table 2). The statistical data on sands were in agreement with those reported on the beaches falling in the same study area [48].

Among the studied beach gravelly sands, only one sample was poorly sorted and polymodal with four modes (Sample TB08, Figure 14b). This significative variability was also related to the presence in the sands of amounts of cartridges of illegal fireworks, accumulated on the beach over several years.

7.2.2. Shape Parameters

The differences among the shape parameters calculated in the beach sands, pebbles, cobbles (BSPC), and technofossils (BT) allowed the author to distinguish them into two different groups. Indeed, the E (Figure 18) and F (Figure 19) parameters were highest in the BSPC and lowest in the BT. The E average values were >0.72–0.76 and <0.72–0.76 in the BSPC and BT, respectively (Figure 18), whereas F was >0.35–0.54 and <0.35–0.54 in the

BSPC and BT, respectively (Figure 19). The lowest average values of E and F were found exclusively in the ACM, as reported in [24]; indeed, E and F were 0.66 and 0.10, respectively. Consequently, as observable in the Zingg diagram (Figure 20), the shapes of the BSPC were mostly from oblate to equant, whereas the shapes of the BT were mostly from bladed to oblate. Analogously to E, the average values of the Riley sphericity analyzed in the beach pebbles and cobbles were higher than in the technofossils (Figure 20).

7.2.3. Average Roundness

The average roundness was elevated (mostly well-rounded and very well-rounded) in all the coarsest materials, natural or anthropogenic (Figure 21). The elevated roundness in the beach pebbles and cobbles (Figure 8), especially the pinkish and grayish porphyroids, could be related to the previous roundness acquired by these clastic particles, part of them being cannibalized rocks from the Pleistocene GSMF. The elevated roundness observed in the technofossils mostly depended on their mechanical behavior, the materials involved being soft, notwithstanding the times of transport being much lower, starting most likely post-World War II. Differently, the average roundness was low in the beach sands, notwithstanding their age. In this case, the angular aspect of the most diffused quartz grains could be directly correlated with the pervasive fractures affecting these grains. This brittle deformation, mostly observed in the quartz grains, could be enhanced by the high energy associated with the drift of the mobile sediments and the particle impacts acting during their transport from the streams to the sea.

The origin of the evident differences in the other main shape parameters observed in the beach pebbles–cobbles and technofossils (Figures 9–12) depended on the original shape of the technofossils, being platy in the natural rock slabs for construction (mostly limestones), bricks, tiles, glass, and ACM, and on composition.

7.3. Hazardous Human-Environmental Relationships

Different concentrations of inorganic anthropogenic wastes were found to be associated with the beach deposits studied in the Tyrrhenian and Ionian beaches. The impressive amounts of hazardous and non-hazardous wastes detected on the Ionian beaches of the Torre Faro locality (Figure 3) evidenced a real ruin, particularly serious falling these beaches into an oriented natural reserve (zone B) and Special Protection Sites, facing into the Messina Strait, a place unique for the beauty of its landscapes and environmental value.

On the Tyrrhenian side, these materials, in order of abundance, were (1) non-hazardous waste made up of bricks, tails, natural rock slabs, and cement (European waste code—CER—170101–03), (2) non-hazardous waste formed of glass (CER 170202), and (3) hazardous waste of ACM (CER 17 06 05*), whereas on the Ionian side, the amount of ACM was much higher and represented the second most abundant waste [24].

The different textural parameters distinguishing the BSPC from the BT represent a significative signature for distinguishing the composition of the natural beach materials from the anthropogenic ones, as well as the different source areas, transport modalities, and time–space evolution.

The peculiar shapes, ornamentations (threads), and colors indicated that the remnants of bricks, tails, slabs, cement (Figure 11), and ACM represented construction and demolition materials, whereas the fragments of glass (Figure 10) could indicate that waste mostly derived from glass bottles of water and beer. Special attention was devoted to individuating the origin of the hazardous waste represented by the ACMs on the basis of their aspects (Figure 12). The evidenced characteristics suggested that the waste mostly derived from eternit slabs for roofing (diffused today in the territory often without any incapsulating paints), water tanks, or tubes (Figure 12f).

The finding of marine encrustations (Figure 12g) grown on previous lichens suggested that part of these materials, after their long stay in continental areas, was also stationed for different years in shallow marine waters, before returning onshore because of the sea waves and winter storms.

The sea-wards and land-wards high mobility of part of the ACM could be dependent on its light specific weight. Notwithstanding, most of the ACM, having very flat shapes, was favored for a long stay on the beach, determining over time a progressive increasing percentage with respect to the igneous and metamorphic pebbles and cobbles. Particularly, the elevated roundness of bricks and ACMs testified to significative abrasion processes due to the marine dynamics. The ACM surfaces were very abraded with well-exposed crocidolite and chrysotile fibers. The exposure to the atmosphere of asbestos fibers may represent a danger for the health of humans and non-human organisms. An analogous issue may be found in the direct contact of humans with the asbestos fibers or their transfer onto footwear, clothing, or beach towels. Due to the high amounts of ACMs on the Ionian coast, this risk is more elevated in the Torre Faro beach where numerous fisher boats are usually moored.

Differently, the angular fragments of ACM were found in the study area in an illegal superficial micro landfill and along the winter berms affecting the beach deposits and underground landfills or abandonments of demolition materials. The illegal landfill, discovered on the Ionian Sea side, was evident because it was eroded by the energy of the waves during sea storms, notwithstanding the important natural defensive action for contrasting the significative coastal erosion exerted by beachrocks. Angular fragments of ACM were also found out of the reserve, about 10 km south, near the Messina town, both on the mouth of the Annunziata stream and along the Ionian Sea-facing slope of the urban park (Parco Sabin) surrounding the right side of the stream (Figures 1 and 23). The park area, used as a landfill of demolition wastes presumably at least since the 1970s–1980s, actually undergoes a strong coastal erosion [50,51] (Figure 23a,b), especially during winter storms, responsible for delivering waste and ACMs into the Ionian Sea.

The source areas for the well-rounded ACMs found in the studied Cape Peloro beaches could have at least four different origins:

i. Possible landfills widespread in the intensively urbanized coastal areas.
ii. Direct abandonment in the coastal area.
iii. Direct abandonment in the streams.
iv. Activities to counteract the erosion/lack of sediment affecting this sector of the coast.

A worrying new recent report described non-conforming materials being used for the contrast of the erosion of a sector of the Ionian coast and the related infrastructure (parking areas), damaged in these last years by wave action. These materials, notwithstanding certification, appeared full of tiles, plastics, and wastes in general [56]. The construction site was seized by the judicial police.

The ACMs were particularly abundant in the Ionian beaches of Messina [24], presumably because the highly urbanized coasts were vulnerable to winter storm action and or coastal erosion (Figure 2a). After their disposal, these materials underwent processes of removal, modeling, and roundness. The average sea wave directions, reported by remote-sensing analyses on satellite imagery [57] and by the PRCEC project [48], were responsible for the actual drift of the mobile sediments, including ACMs, parallel to the Ionian coastline and mostly NE-wards (Figure 2b).

A temporal analysis on the ACM contamination of the study coasts is underway, notwithstanding preliminary historical information, provided by interviews with old civil workers, reported that part of the Messina Ionian coasts, from S to N of the city center, could experience the uncontrolled abandonment of demolition materials, ACMs included, since the 1970s.

As regards the Tyrrhenian coast of the study area, the amount of ACM was significative but in minor amounts with respect to the Ionian side, as reported in previous research [24]. It must be underlined that the area being less impacted by the urbanization could have the benefit of a lower anthropogenic stress. In this case, the (ii) and (iii) origins could nourish the sediment drift, parallel to the coast and mainly directed east-wards (Figure 2).

Preliminary surveys made during a storm event, west-wards, out of the reserve, at the Cape Orlando beach (about 80 km west of Cape Peloro), indicated an absence of ACM.

It must be evidenced that other hazardouswastes present locally in the Cape Peloro reserve are represented by the cartridges of fireworks abandoned on the beach. Indeed, in general, there is a growing phenomenon of exploding fireworks during private parties in nightclubs, usually at midnight [58]. In the present case, the cartridges were found on the beach. These unauthorized activities, beyond causing acoustic pollution (with consequent inconveniences for human and non-humans), simultaneously created several illegal abandonments, being cartridges expensive to dispose.

8. Conclusions

The unsuccess of the reclamation activities carried out in these years in different Italian regions (Sardinia) [59] evidenced that the simple manual removal of ACMs from the beach or the remobilization of sands by means of mechanical excavators cannot be sufficient actions for contrasting or solving this growing problem. Marine coastal plains and beaches are complex dynamic systems that actually may be strongly modified by erosion and accretion phenomena. Consequently, ACMs being included in the beach deposits and also coming from submerged areas [24] evidently cannot be eliminated in such a simple way. Effective reclamation activities of ACM-contaminated environments should consider several different crucial aspects for providing permanent results. Three of them should be the main pillars of conceptual models at the base of possible reclamation activities:

i. The extent of the contaminated beach deposits (in surface and depth).
ii. The source of the contaminant sources.
iii. The main mechanisms responsible for the contaminant dispersion.

As regards the epidemiological issue, according to the VII report of the Italian national mesothelioma registry of 2021, there are 31,572 (calculated according to the number of villages) cases of mesothelioma in the country [24,60]. The origin of the exposure is unknown for 17.4% of the national cases. Among these, the populations of Messina, Catania, and Palermo show the highest incidence of mesothelioma with respect to the Sicilian region [24,60]. Notwithstanding, it must be underlined that actually there are no epidemiological and environmental data inferring the unknown exposure mesothelioma cases in Messina to the ACMs found in the beaches. Indeed, the unknown exposure to asbestos fibers could be dependent on the ACMs present on the beaches, as well as on other sources such as asbestos present in the roofs of old houses or in working sites. However it may be, due to the long time to manifest asbestos-related disease, the incidence of mesothelioma should decrease with an age-standardized rate of 20–40 years [24,60].

On the basis of the above, for a protection precautionary principle, competent organizations for the protection of the human and animal health and environment should pay attention to this growing phenomenon of environmental contamination.

It is desirable that the research presented here, together that reported in [23,24], may provide to other scientists, as well as to managers, politicians, and officials, effectual scientific data for correctly planning the following in the future: (i) efficient removal and reclamation activities for limiting possible health and environmental damages, (ii) regulatory measures, and (iii) guidelines to prevent further contamination.

Funding: This research received no external funding.

Acknowledgments: The author is grateful to Giovanna D'Angelo and Rosaria Verduci (University of Messina) for having allowed the author to report some preliminary data on the spectroscopic analyses on heavy minerals, performed for a study in progress. The author wants to reserve a special and deep acknowledgement to Maria Molino (director of the oriented reserve of Cape Peloro, Metropolitan City of Messina) for allowing the author to accomplish the sampling activities related to the scientific research on the beaches of the Cape Peloro reserve. The author is also thankful to the three anonymous reviewers and the academic editor that assisted the author in strongly improving the quality of the present research.

Conflicts of Interest: The author declares no conflicts of interest.

References

1. Legambiente. Available online: https://www.legambiente.it/rapporti-e-osservatori/liberi-dallamianto/ (accessed on 2 February 2024).
2. Osservatorio Nazionale Amianto. Available online: https://onanotiziarioamianto.it/amianto-spiagge-necessario-effettuare-bonifica/ (accessed on 2 February 2024).
3. Il Secolo XIX. Available online: https://www.ilsecoloxix.it/imperia/2013/05/09/news/amianto-emergenza-in-spiaggia-1.32312548 (accessed on 2 February 2024).
4. Gruppo d'Intervento Giuridico. Associazione Ecologista. Available online: https://gruppodinterventogiuridicoweb.com/2022/05/15/cagliari-bonificata-dai-detriti-di-amianto-la-spiaggia-del-poetto/ (accessed on 20 December 2023).
5. La Nuova di Venezia e Mestre. Available online: https://nuovavenezia.gelocal.it/venezia/cronaca/2010/01/21/news/venezia-quintali-di-eternit-nella-cittadella-del-cinema-1.1337278 (accessed on 3 December 2023).
6. GalluraOggi.it. Available online: https://www.galluraoggi.it/cronaca/eternit-marina-maria-bonifiche-spiaggia-2-aprile-2023/ (accessed on 30 December 2023).
7. LinkOristano. Available online: https://www.linkoristano.it/2020/06/11/bene-la-pulizia-della-spiaggia-ad-abarossa-ce-ancora-amianto/ (accessed on 30 December 2023).
8. RomaToday. Available online: https://www.romatoday.it/cronaca/amianto-via-del-pesce-luna-fiumicino.html (accessed on 30 December 2023).
9. FondiNotizie.net. Available online: https://www.fondinotizie.net/notizie/territorio/52/una-spiaggia-fatta-di-amianto#google_vignette (accessed on 30 December 2023).
10. La Nazione. Available online: https://www.lanazione.it/viareggio/cronaca/eternit-spiaggia-libera-c9217e92 (accessed on 27 December 2023).
11. Il Tirreno. Available online: https://www.iltirreno.it/piombino/cronaca/2018/04/23/news/eternit-sulla-spiaggia-della-sterpaia-1.16748868 (accessed on 28 December 2023).
12. LaRegione. Available online: https://www.laregione.ch/estero/estero/1602113/lastre-eternit-lucca-viareggio-ambiente (accessed on 15 December 2023).
13. QuiCosenza. Available online: https://www.quicosenza.it/news/provincia/42898-ancora-amianto-sul-litorale-di-san-lucido-spiagge-sotto-sequestro (accessed on 5 December 2023).
14. BrindisiReport. Available online: https://www.brindisireport.it/cronaca/frammenti-di-Eternit-abbandonati-da-anni-su-spiaggia-di-Specchiolla.html (accessed on 15 December 2023).
15. OsservatorioOggi. Available online: http://www.osservatoriooggi.it/notizie/attualita/5694-amianto-torre-cane-spiaggia-bambini-turisti-fasano (accessed on 15 February 2024).
16. Ilnuovoamico. Available online: https://www.ilnuovoamico.it/2018/07/amianto-pericolo-a-ridosso-della-spiaggia-di-pesaro/ (accessed on 15 February 2024).
17. Livesicilia. Available online: https://livesicilia.it/amianto-seppellito-sotto-la-sabbia-bonifica-alla-spiaggia-numero-3/ (accessed on 15 February 2024).
18. Normanno. Available online: https://normanno.com/attualita/lastre-amianto-due-passi-dal-mare-biancuzzo-vanno-rimosse-subito/ (accessed on 15 February 2024).
19. Tempostretto. Available online: https://www.tempostretto.it/news/inquinamento-sabbia-eternit-tanto-mare-sant-agata-mortelle.html (accessed on 15 February 2024).
20. Messinatoday. Available online: https://www.messinatoday.it/cronaca/indagini-spiaggia-mili-marina-rifiuti-amianto-.html (accessed on 15 February 2024).
21. La Repubblica. Available online: https://www.repubblica.it/green-and-blue/2010/05/03/news/spiagge_d_amianto_sui_fiumi_italiani_il_wwf_il_po_usato_come_discarica_-267371981/ (accessed on 22 February 2024).
22. WWF Italia. Available online: https://www.wwf.it/pandanews/ambiente/amianto-nella-campagne-blitz-delle-guardie-wwf/ (accessed on 5 April 2024).
23. Lisco, S.; Lapietra, I.; Laviano, R.; Mastronuzzi, G.; Fracchiolla, T.; Moretti, M. Sedimentological features of asbestos cement fragments in coastal environments (Taranto, southern Italy). *Mar. Pollut. Bull.* **2023**, *187*, 114469. [CrossRef]
24. Somma, R.; Giacobbe, S.; La Monica, F.P.; Molino, M.L.; Morabito, M.; Spoto, S.E.; Zaccaro, S.; Zaffino, G. Defense and protection of the marine coastal areas and human health: A case study of asbestos cement contamination (Italy). *Geosciences* **2024**, *14*, 98. [CrossRef]
25. Ispra Ambiente. Available online: https://www.isprambiente.gov.it/files/pubblicazioni/statoambiente/tematiche2011/05_%20Mare_e_ambiente_costiero_2011.pdf (accessed on 22 February 2024).
26. Zalasiewicz, J.; Williams, M.; Waters, C.N.; Barnosky, A.D.; Haff, P. The technofossil record of humans. *Anthr. Rev.* **2014**, *1*, 34–43. [CrossRef]
27. Messina, A.; Somma, R.; Macaione, E.; Carbone, G.; Careri, G. Peloritani continental crust composition (southern Italy): Geological and petrochemical evidence. *Boll. Soc. Geol. Ital.* **2004**, *123*, 405–441.

28. Regione Sicilia. Available online: https://www.regione.sicilia.it/sites/default/files/2024-01/Format%20ITA030042-%20Monti%20Peloritani,%20Dorsale%20Curcuraci,%20Antennamare%20e%20area%20marina%20dello%20stretto%20di%20Messina.pdf (accessed on 2 January 2024).
29. Regione Sicilia. Available online: https://www.regione.sicilia.it/sites/default/files/2024-01/Format%20ITA030008%20-%20Capo%20Peloro%20-%20Laghi%20di%20Ganzirri.pdf (accessed on 15 February 2024).
30. National Geographic. Available online: https://www.nationalgeographic.co.uk/travel/2022/08/12-of-the-best-beaches-in-italy (accessed on 2 January 2024).
31. Bonardi, G.; Giunta, G.; Liguori, V.; Perrone, V.; Russo, M.; Zuppetta, A. Schema geologico dei Monti Peloritani. *Boll. Soc. Geol. It.* **1976**, *95*, 49–74.
32. Bonardi, G.; Caggianelli, A.; Critelli, S.; Messina, A.; Perrone, V.; Acquafredda, P.; Carbone, G.; Careri, G.; Cirrincione, R.; Derrico, M.; et al. Geotraverse across the Calabria-Peloritani Terrane (Southern Italy). In Proceedings of the 32nd International Geological Congress IUGS, Florence, Italy, 20–28 August 2004; Servizio Geologico d'Italia—APAT: Rome, Italy, 2004; pp. 1–60.
33. Atzori, P.; Cirrincione, R.; Del Moro, A.; Pezzino, A. Structural, metamorphic and geochronologic features of the Alpine event in south-eastern sector of the Peloritani Mountains (Sicily). *Period. Mineral.* **1994**, *63*, 113–125.
34. Cirrincione, R.; Pezzino, A. Caratteri strutturali dell'evento alpino nella serie mesozoica di Alì e nell'unità metamorfica di Mandanici (Peloritani orientali). *Mem. Soc. Geol. Ital.* **1991**, *47*, 263–272.
35. Bonardi, G.; Compagnoni, R.; Del Moro, A.; Macaione, E.; Messina, A.; Perrone, V. Rb–Sr age constraints on the Alpine metamorphic overprint in the Aspromonte nappe (Calabria–Peloritani composite terrane, southern Italy). *Boll. Della Soc. Geol. Ital.* **2008**, *127*, 173–190.
36. Somma, R.; Martin Rojas, I.; Perrone, V. The stratigraphic record of the Alì-Montagnareale Unit (Peloritani Mountains, NE Sicily). *Rend. Online Soc. Geol. Ital.* **2013**, *25*, 106–115.
37. Guerrera, F.; Wezel, F.C. Nuovi dati stratigrafici sui flysch oligomiocenici siciliani e considerazioni tettoniche relative. *Riv. Mineraria Sicil.* **1974**, *147*, 27–51.
38. Carbone, S.; Messina, A.; Lentini, F.; Barbano, M.S.; Grasso, D.; Di Stefano, A.; Ferrara, V.; Somma, R. *Note Illustrative della Carta Geologica D'italia alla Scala 1: 50.000: Foglio 601*; Dipartimento Difesa del Suolo, Servizio Geologico d'Italia: Firenze, Italy, 2008; pp. 1–170.
39. Segre, A.G.; Bagnala, R.; Sylos Labini, S. Holocene evolution of the Pelorus headland, Sicily. *Quat. Nova* **2004**, *8*, 69–78.
40. Catalano, S.; Cirrincione, R.; Mazzoleni, P.; Pavano, F.; Pezzino, A.; Romagnoli, G.; Tortorici, G. The effects of a Meso-Alpine collision event on the tectono-metamorphic evolution of the Peloritani mountain belt (eastern Sicily, southern Italy). *Geol. Mag.* **2018**, *155*, 422–437. [CrossRef]
41. Guarnieri, P.; Pirrotta, C. The response of drainage basins to the late Quaternary tectonics in the Sicilian side of the Messina Strait (NE Sicily). *Geomorphology* **2008**, *95*, 260–273. [CrossRef]
42. Ministero delle Infrastrutture e della Mobilità Sostenibili. Available online: https://www.google.com/search?q=relazione+geologica+ponte+sullo+stretto&rlz=1C1FHFK_itIT958IT958&oq=relazione+geologica+ponte+sullo+stretto&gs_lcrp=EgZjaHJvb-WUyBggAEEUYOdIBCjEzNDkwajBqMTWoAgCwAgA&sourceid=chrome&ie=UTF-8 (accessed on 26 February 2024).
43. Antonioli, F.; Ferranti, L.; Lambeck, K.; Kershaw, S.; Verrubbi, V.; Dai Pra, G. Late Pleistocene to Holocene record of changing uplift rates in southern Calabria and northeastern Sicily (southern Italy, Central Mediterranean Sea). *Tectonophysics* **2006**, *422*, 23–40. [CrossRef]
44. Danjo, T.; Kawasaki, S. Characteristics of beachrocks: A review. *Geotech. Geol. Eng.* **2014**, *32*, 215–246. [CrossRef]
45. Regione Siciliana. Available online: https://www.sitr.regione.sicilia.it/pai-coste-sicilia-e-aggiornamento-dati-pai/ (accessed on 27 February 2024).
46. Regione Siciliana. Available online: https://www.regione.sicilia.it/sites/default/files/2021-09/01%20-%20D.A.%20319%20del%205%20agosto%202016%20(ARTA)%20-%20Utilizzo%20Aree%20demani.pdf (accessed on 27 February 2024).
47. Regione Siciliana. Available online: https://www2.regione.sicilia.it/presidenza/ucomrifiuti/acque/DOCUMENTI/DOCUMENTI_D/D2/Acque_costiere.pdf (accessed on 27 February 2024).
48. Regione Sicilia. Available online: https://www2.regione.sicilia.it/deliberegiunta/file/giunta/allegati/N.290_16.07.2020.pdf (accessed on 27 February 2024).
49. Randazzo, G.; Cigala, C.; Crupi, A.; Lanza, S. The natural causes of shoreline evolution of Capo Peloro, the northernmost point of Sicily (Italy). *J. Coast. Res.* **2014**, *70*, 199–204. [CrossRef]
50. Folk, R.L.; Ward, W.C. Brazos River Bar—A study in the significance of grain size parameters. *J. Sediment. Petrol.* **1957**, *27*, 3–26. [CrossRef]
51. Blott, S.J.; Croft, D.J.; Pye, K.; Saye, S.E.; Wilson, H.E. Particle size analysis by laser diffraction. *Geol. Soc. Spec. Publ.* **2004**, *232*, 63–73. [CrossRef]
52. Eshel, G.; Levy, G.J.; Mingelgrin, U.; Singer, M.J. Critical Evaluation of the Use of Laser Diffraction for Particle-Size Distribution Analysis. *Soil Sci. Soc. Am. J.* **2004**, *68*, 736–743. [CrossRef]
53. Lucchi, F.R.; Mutti, E. *Sedimentologia*; Parte I, II, III; Clueb: Bologna, Italy, 1980.
54. Perri, F.; Dominici, R.; Le Pera, E.; Chiocci, F.L.; Martorelli, E. Holocene sediments of the Messina Strait (southern Italy): Relationships between source area and depositional basin. *Mar. Pet. Geol.* **2016**, *77*, 553–566. [CrossRef]

55. Sánchez-Navas, A.; Macaione, E.; De Cassia Oliveira-Barbosa, R.; Messina, A.; Martín-Algarra, A. Transformation of kyanite to andalusite in the Benamocarra Unit (Betic Cordillera, S. Spain). Kinetics and petrological significance. *Eur. J. Mineral.* **2016**, *28*, 337–353. [CrossRef]
56. Gazzetta del Sud. Available online: https://rtp.gazzettadelsud.it/programmi/telegiornale/2024/05/11/lo-stop-ai-lavori-del-parcheggio-paradiso-di-messina-la-sabbia-con-plastica-era-certificata-come-idonea-454d238c-204c-4b03-8f8f-860b302faf6a/ (accessed on 11 May 2024).
57. Copernicus. Available online: https://marine.copernicus.eu/ (accessed on 27 February 2024).
58. Gazzetta del Sud. Available online: https://rtp.gazzettadelsud.it/programmi/telegiornale/2024/04/22/messina-fuochi-dartificio-illegali-a-mezzanotte-un-malcostume-da-perseguire-7279ea12-aa01-40be-a2a5-01cfed6a745b/#:~:text=Una%20clamorosa%20bufala%20che%20non,o%20altre%20ricorrenze%20del%20genere (accessed on 24 April 2024).
59. Gruppo d'Intervento Giuridico. Available online: https://gruppodinterventogiuridicoweb.com/2022/04/07/nuovamente-amianto-sulla-spiaggia-del-poetto-cagliari/ (accessed on 30 April 2024).
60. VII Rapporto del Registro Nazionale dei Mesoteliomi (ReNaM), Italia. 2021. Available online: https://www.inail.it/cs/internet/comunicazione/pubblicazioni/catalogo-generale/pubbl-il-registro-nazionale-mesoteliomi-settimo-rapporto.html (accessed on 30 April 2024).